Anton Buchberger, BSc

Development and characterization of a humidity measurement system based on polymeric hydrogels

MASTER'S THESIS

to achieve the university degree of

Diplom-Ingenieur

Master's degree programme: Technical Physics

submitted to

Graz University of Technology

Supervisor

Assoc.Prof. Dr. Anna Maria Coclite

Institute of Solid State Physics

Co-Supervisor
Univ.-Prof. Mag.rer.nat. Dr.rer.nat. Alexander Bergmann

Graz, March 2018

AFFIDAVIT

I declare that I have authored this thesis independently, that I have not used other than the declared sources/resources, and that I have explicitly indicated all material which has been quoted either literally or by content from the sources used. The text document uploaded to TUGRAZonline is identical to the present master's thesis.

_____   _____
Date   Signature

Acknowledgment

Abstract

The field of humidity sensing is constituted by various measurement principles, that are adjusted to their application. The focus of this work is the development of an industrial applicable, fast humidity sensor, that is usable also in harsh environment. Many commercially available sensors are based on the change of capacitance in an electronic circuit and rather slow. An application in explosive or corrosive environment is not possible in most cases.

The newly developed measurement system is based on the thickness change of a hydrogel thin film, that is dependent on the relative humidity level of the ambient air. The swellability is described by the Flory-Huggins theory, that directly relates the swelling ratio (initial over swollen thickness) of the hydrogel to the RH level. The thickness of the hydrogel lies in the order of a few hundred nanometers. Two measurement principles have been designed and implemented, that are based on interference phenomena of visible light.

The first approach consists of a laser and a photo detector and is designed to measure relative thickness changes. Unexpectedly intense swelling of the thin film over the applied humidity range causes some ambiguities in the evaluation. It is not possible to map from a measured intensity to a unique thickness value. However, the response times to an abrupt change of the humidity level could be still evaluated for $RH < 60\%$. A common measure is the 63% time constant for the observed exponential response signal, which is $\tau_{63,pow} = (1.5 \pm 0.5)\,\mathrm{s}$ for an abrupt signal increase and $\tau_{63,pow} = (2.5 \pm 0.5)\,\mathrm{s}$ for the corresponding decrease, applied to the thin film.

The thickness measurement based on the second method is implemented with a broadband light source and a spectrometer and yields to absolute values. This information is derived by a fit of the interference pattern, which is observed in the measured reflectance spectrum and uniquely dependent on the thickness. With this data, a further investigation of the Flory-Huggins theory could be performed. It contains the so called Flory-Huggins parameter χ, that is dependent on the water concentration of the hydrogel and thus on the thickness ratio and RH level respectively. By simultaneous measurement of RH and fit with a polynomial expansion, the Flory-Huggins parameter χ for a pure pHEMA (Poly 2-hydroxyethyl methacrylate) thin film could be derived in a volume fraction range of the hydrogel with water from 0.45 to 1. The application of this approximation to the Flory-Huggins theory enables the conversion of measured thickness ratios to RH values for any pure pHEMA thin film. This is an important outcome for future sensor applications. Evaluation measurements, performed with the actual setup, show reasonable and promising results. However, there is still some improvement to be done, like the material composition of the hydrogel in order to achieve better linearity of the swelling and improve the overall sensitivity of the sensor.

There is an ongoing project where the measurement principle is implemented as a fiber version. Measurements in harsh and even explosive environment will be possible with this robust sensor setup.

Zusammenfassung

Angepasst an die jeweilige Anwendung, umfassen eine Reihe unterschiedlicher Messprinzipien das Gebiet der Luftfeuchtigkeitsmessung. Der Fokus dieser Arbeit liegt auf der Entwicklung eines industriell einsetzbaren, schnellen Feuchtesensors, der auch in rauen Umgebungen verwendet werden kann. Ein Großteil der im Handel erhältlichen Sensoren basiert auf der Kapazitätsänderung in einer elektronischen Schaltung und reagiert eher langsam. Eine Anwendung in explosiver oder korrosiver Umgebung ist in den meisten Fällen nicht möglich.

Das neu entwickelte Messsystem basiert auf der Dickenänderung eines Hydrogel-Dünnfilms, die von der relativen Luftfeuchtigkeit der Umgebungsluft abhängt. Die Quellbarkeit wird durch die Flory-Huggins-Theorie beschrieben, wobei die relative Luftfeuchtigkeit eine direkte Funktion des Quellungsverhältnisses (anfängliche zu geschwollene Dicke) des Hydrogels ist. Die Dicke des Dünnfilms liegt bei einigen hundert Nanometern. Es wurden zwei Messprinzipien umgesetzt, die auf Interferenzphänomenen des sichtbaren Lichts basieren.

Das erste Prinzip ist mit einem Laser und einem Photodetektor aufgebaut um relative Dickenänderungen zu messen. Durch unerwartet starkes Anschwellen des Hydrogels ist eine eindeutige Zuordnung von einem gemessenen Intensitätswert zur relativen Dicke bei hohen Feuchtigkeiten nicht möglich. Dennoch können die Reaktionszeiten auf eine abrupte Änderung des Feuchtigkeitsniveaus für $RH < 60\,\%$ ausgewertet werden. Ein übliches Maß dafür ist die $63\,\%$ Zeitkonstante für das beobachtete, exponentielle Antwortsignal, die $\tau_{63,pow} = (1.5 \pm 0.5)\,\mathrm{s}$ für eine abrupte Zunahme und $\tau_{63,pow} = (2.5 \pm 0.5)\,\mathrm{s}$ für die entsprechende Abnahme der Dünnschicht ist.

Die Dickenmessung nach der zweiten Methode besteht aus einer breibandigen Lichtquelle und einem Spektrometer und führt zu absoluten Werten. Diese Information wird durch einen Fit des im gemessenen Reflexionsspektrum beobachteten Interferenzmusters ermittelt, der eindeutig von der Dicke abhängt. Mit diesen Daten kann eine detailliertere Untersuchung der Flory-Huggins-Theorie durchgeführt werden. Sie enthält den sogenannten Flory-Huggins-Parameter χ, der von der Wasserkonzentration des Hydrogels und damit vom Dickenverhältnis bzw. vom RH Level abhängt. Durch gleichzeitige Messung von RH und Schichtdicke wurde mittels Fit einer Polynomentwicklung im Bereich von 0.45 bis 1 des Volumenanteils des Hydrogels mit Wasser der Flory-Huggins Parameter χ für einen reinen pHEMA (Poly 2-Hydroxyethylmethacrylat) Dünnfilm ermittelt. Nach Einsetzen dieser Näherung in die Flory-Huggins-Modellfunktion ist es möglich, gemessene Dickenverhältnisse auf RH Werte umzurechnen. Dies ist ein Ergebnis, das für jeden reinen pHEMA-Dünnfilm gültig ist und bildet die Basis für zukünftige Sensoranwendungen. Grundsätzlich führen die mit dem Setup durchgeführten Evaluierungsmessungen zu vielversprechenden Ergebnissen. Nichtsdestotrotz gibt es Raum für Verbesserungen, beispielsweise in der Materialzusammenstellung des Hydrogels. Eine Materialkonfiguration deren Quellungsverhalten linearer ausgeprägt ist, wäre für die Messempfindlichkeit über den gesamten Feuchtigkeitsbereich von Vorteil.

Weiters wurde ein Projekt gestartet, in welchem der Messaufbau als Lichtfaser implementiert ist. Mit diesem robusten Setup werden Messungen in rauer und sogar explosionsgefährdeter Umgebung möglich.

Contents

1 Introduction

Water is the basis for life. All organisms contain 50–90 % water and some aquatic organisms even 99 %. It is involved in many processes of life and the climate system as well [1]. For processes in the climate system, water in the atmosphere plays an important role, where it occurs in two different forms. The term moisture refers to the amount of liquid water in a gas in form of small droplets, whereas by humidity the amount of gaseous water is meant [2].

1.1 Terminology

There are various physical quantities, which describe humidity (from [3]):

Absolute humidity AH equals the total mass of water vapor (gas phase) present in a given mass of air. If ideal gas behavior is assumed, the following applies.

$$AH = \frac{M_w p}{M_a (P - p)} \tag{1}$$

AH ... absolute humidity; M_w, M_a ... molecular weight of water, air; p ... partial pressure of water vapor; P ... total pressure

Saturation humidity H_s is the absolute humidity, when the partial pressure p of water vapor in the air at a given temperature equals the equilibrium vapor pressure of water p_s at the same temperature. This means the air is saturated.

Relative humidity RH is defined as the ratio of the partial pressure p of water vapor in the air, over the equilibrium vapor pressure p_s of water at the given temperature.

$$RH = \frac{p}{p_s} \tag{2}$$

Since the equilibrium vapor pressure p_s is temperature dependent, also the relative humidity RH is a temperature dependent quantity. Thus, RH values are just comparable, if the temperature is known. In most cases RH is specified as a percentage.

Dew point temperature (or saturation temperature) is the temperature when saturation occurs, meaning when a given mixture of water vapor and air is saturated. The water equilibrium vapor pressure is equal to the partial pressure of water vapor in this condition. If the temperature is further decreased, water starts to condensate.

1.2 Humidity Measurement

A very important application of humidity measurement is meteorology. It indicates the likelihood for phenomena like precipitation, dew or fog. There are several other fields of science and industry, where humidity measurements play an important role, ranging from monitoring gas flows in industrial processes to medical investigations like breath recording [2]. For measuring humidity, a commonly used quantity is the percentage relative humidity RH. Most commercially available systems are based

on the measurement of a quantity, that is dependent on the absolute water content and compute the corresponding RH value. A temperature measurement is needed for relating the data to the actual equilibrium vapor pressure. Another possible output is the dew point temperature, that refers to the temperature, at which the gas mixture is saturated. In contrast to the relative humidity, the dew point is easier to compare, because it refers to the absolute amount of water in the air. The dew point is an suitable indicator of the level of human discomfort in warm, humid weather. When the dew point rises above 20 °C, people start to feel uncomfortable. Whereas a relative humidity of 70 %RH may feel quite comfortable at 20 °C, it would cause considerable discomfort at 30 °C [4].

1.2.1 Classical Hygrometers

Hygrometers are devices for measuring the humidity, which refers to the amount of water vapor in the air.

The first hair-tension hygrometer was built already in 1783 by the Swiss physicist and geologist Horace Bénédict de Saussure. „It consists of a human hair eight to ten inches long, fastened at one extremity to a screw and at the other passing over a pulley being strained tight by a silk thread and weight“ [5]. It is possible to measure the change in length with an attached graduated scale, when the hygroscopic hair is exposed to humid air. Even if this sounds like an ancient method, there are still modern devices like hygrographs based on this principle. Also the traditional weather houses, that are popular in the area of the Alps, use the same effect [6].

Psychrometers are another class of hygrometers. They basically consist of two thermometers exposed side by side. The surface of the sensing element of one thermometer is covered by a thin film of water and termed the wet bulb. The dry bulb is the second thermometer, with the sensing element exposed to air. In general, the temperature measured by the wet-bulb thermometer is lower than that one measured with the dry bulb, due to evaporation. The temperature difference is a measure of the humidity in the air. This method is commonly used for observational purposes and instruments based on that principle are applied as working standards [7].

Chilled dew point hygrometers detect directly the dew point by condensation at a cooled surface. Common systems employ a small polished metal reflecting surface, which is cooled electrically using the Peltier effect. The condensation is sensed with an optical detector. Such instruments are used for observational purposes and are also possible working standards and/or reference standards [7].

The gravimetric method is a measure of the absolute water-vapor content of the air in terms of its humidity mixing ratio. First the water vapor is removed from the sample gas. By weighing the drying agent before and after absorbing the vapor, the mass of the water vapor is determined [7]. Gravimetric methods represent the most accurate way of measuring humidity and therefore such devices are used for comparison and calibration of lower order standard instruments [8].

1.2.2 Modern Hygrometers

Capacitive humidity sensors are widely used in industrial, commercial and meteorological applications. They are based on the change of the dielectric constant of a polymer or metal oxide thin film layer, which is almost directly proportional [9]. A typical uncertainty of those type of sensors is $\pm 2\,\%$RH and the lowest response time τ_{63} is about $8\,\mathrm{s}$ [10].

Resistive humidity sensors are made of a hygroscopic medium such as a conductive polymer, salt or treated substrate and measure the change in electrical impedance, which is typically an inverse exponential relationship to humidity. When the sensor material absorbs water vapor, ionic functional groups are dissociated and the electrical conductivity is increased. Compared to capacitive sensors, the typical uncertainty is similar (about $\pm 2\,\%$) and the response times are a slightly higher (between 10 to $30\,\mathrm{s}$) [9].

Acoustic methods for measuring humidity are developed more recently. There is actual research done applying the photo-acoustic effect, which is based on absorption of light, that is followed by the formation of sound waves of water molecules [11]. Other methods, that employ an acoustic effect, did not leave the experimental stage either and have not led to the development of new sensors yet [2].

Optical sensors have emerged with the development of fiber technologies. These sensors, which are mainly based on interferometric techniques, are faster and more robust than the electronic ones. Today, humidity sensors based on fiber interferometers are still relatively costly in comparison with electronic ones, but they provide some important advantages. For example, they are applicable in explosive environments like in chemical industry or in gas pipelines, because of the lack of electricity in the sensor head. The response times of optical sensors are better than the electronic ones, which makes them interesting for high dynamic measurements, that would not be possible with conventional methods (e.g. breath monitoring) [2, 12].

2 Motivation

Depending on the application, different humidity measurement systems are important. Response times in the order of minutes would be all right in meteorology, but especially in industrial process monitoring or in medical applications such response times could be already too high. Furthermore, in some applications cross-sensitivities with other gases have to be dealt with. According to *Konrad Peterka*, who is manager at OÖ. Ferngas Netz GmbH (gas supplying company), water content monitoring inside gas pipelines with state-of-the-art capacitative humidity sensors is an actual problem. Occasional appearing glycerin may saturate the applied sensor and inhibit the water monitoring. The explosive environment limits the range of applicable sensor systems further. Another possible application of a robust measurement system is the approach of predicting corrosion of reinforcement rods in concrete. The amount of water in the vicinity of the rods within the concrete could be a promising indicator. A fiber optic based humidity sensor would be a possible setup, that withstands the challenges in such a corrosive environment.

New materials and measurement techniques are under development to tackle these challenging tasks. A promising class of materials are hydrophilic polymer networks, the so-called hydrogels. The group of *Anna Maria Coclite*, from the *Institute for Solid State Physics* at *TU Graz*, deals with such materials and is focused on different deposition methods. In former work it is shown, that Poly 2-hydroxyethyl methacrylate (pHEMA), deposited with a method called initiated chemical vapor deposition (iCVD), has an excellent swelling behavior. It increases its thickness related to the humidity in the surrounding atmosphere [13]. A humidity sensor could be created by optical detection of this effect. This device could provide fast response times and a good applicability also in harsh environment, where electronic sensors would fail.

2.1 Objective

Considering the motivation that is described above, the objective of this Master's thesis is the following:

> *Development and characterization of an industrially applicable, fast humidity measurement system, based on the thickness change of a polymeric hydrogel thin film (pHEMA), as a proof of concept.*

For achieving this goal, the project is separated into three different parts:

1. Setting up a stable humidity generator with high dynamic properties

2. Conception and realization of a sufficiently fast thin film thickness measurement setup

3. Definition of an appropriate material composition and deposition of the hydrogel

According to the workload of the whole project, it was decided to divide it into two separate theses. This work is about the measurement setup and the humidity generator, whereas the second thesis realized by *Sebastian Peterka* is focused on the materials composition and deposition process of the hydrogel thin film.

2.2 Requirements

Since the measurement system is meant to become an industrial applicable sensor, there are a few boundary conditions that need to be satisfied. The system should work without using any kind of ionizing radiation. Established thin film measurement techniques like X-Ray reflectivity (XRR) are therefore not possible. Costs and dimensions are further crucial factors. Thus, also ellipsometry is not a possible method due to its bulkiness and expenses. Another criterion is the possibility of measuring the thickness from the backside of a substrate, in order to avoid any parts on the side of the hydrogel thin film coating, that would hinder the access of water vapor to the surface. For the investigation of the expected fast response of the hydrogel layer, the sampling rate of the measurement system must be high enough. Including all these requirements a setup is chosen, that measures the interference signal of a multiply reflected laser beam.

3 Theory

Former work has shown, that the thickness of a pHEMA thin film relatively changes with variation of the ambient RH level. It is described by the Flory-Huggins theory, that applies for hydrogels [13]. With this model it is sufficient to measure just a relative change in thickness, if the initial value is known. This can be achieved by measuring a reflected laser interference signal.

3.1 Hydrogels

The *International Union of Pure and Applied Chemistry* (IUPAC) defines a gel as a „non-fluid colloidal or polymer network, that is expanded throughout its whole volume by a fluid" [14]. A gel becomes softer, if more solvent is added, but owing to the permanent bonds, that connect the chains, it always remains a solid [15]. Different forms of gels are common in everyday life, ranging from personal care products to food. Nature has also developed gel-like structures to create unique properties for macrobiological systems, like spider webs or the vitreous humor of eyes [16]. Hydrogels are a special group of this class of materials. A common description defines a hydrogel as „a water-swollen, and cross-linked polymeric network produced by the simple reaction of one or more monomers" [17]. Poly 2-hydroxyethyl methacrylate (pHEMA) is a representative of this group and was of great importance already in the 1970s. It was one of the first materials for soft contact lenses as a co-polymer with ethylene glycol dimethacrylate (EGDMA) and termed *Polymacon* [18]. However, also currently it is an active field of research, because it has potential as a biomaterial, that does not show any toxic or carcinogenic effects [19, 20]. In general, the mechanical properties of hydrogels show interesting features. One of them is their ability to change volume manifold, when exposed to water. The volume fraction ϕ of the polymer in a swollen state can be easily determined experimentally by measuring the volume V of the hydrogel (including water) and its volume in the dry state V_{dry}, described by equation (3) [15]. This assumes that the total amount of polymer in a well-developed hydrogel does not change during swelling or deswelling and the change of the volume is entirely due to a variation of the amount of water within the gel.

$$\phi = \frac{V_{dry}}{V} \tag{3}$$

ϕ ... volume fraction; V ... volume in the swollen state; V_{dry} ... volume of the dry state

If the hydrogel is unconstrained, it undergoes uniform swelling by the same amount in all directions. During a swelling process, all the network strands are stretched as the crosslink junctions move further apart. The stretching can be described by an ideal chain model with freely jointed rods, that result in a distribution of end-to-end vectors of the chains, based on a random walk treatment. Considering the entropy of a freely jointed chain, this leads to a modulus of the hydrogel, determined by the elastic free energy per chain. „At swelling equilibrium, the elasticity is balanced by the osmotic pressure Π of a semidilute solution of uncrosslinked chains at the same concentration. Since the modulus is proportional to the elastic free energy per unit volume, any hydrogel swells until modulus and osmotic pressure are balanced" [15].

Hydrogels can be described by a binary mixing model as a polymer solution. Those mixtures consist only of two different species, namely the polymer and the solvent, which is water in this case. In most experimental situations mixing occurs at constant pressure and the enthalpic interactions between species must be analyzed to find a minimum of the free energy of mixing [15].

3.1.1 Flory Huggins Theory

Gas sorption by a non-polar or weakly polar polymer can be regarded as a dissolution process analogous to that in liquid solvents and can be described by regular solution theory, the so-called Flory Huggins theory [21, 22]. In this simplified lattice model, components are mixed at constant volume and therefore the Helmholtz free energy $\Delta \bar{F}_{mix}$ (natural variables T,V) of mixing is relevant, which contains an energetic and entropic part (equation (4)). The bar denotes a definition *per lattice site* (intensive property).

$$\Delta \bar{F}_{mix} = \Delta \bar{U}_{mix} - T \Delta \bar{S}_{mix} \tag{4}$$

with the entropic part $\Delta \bar{S}_{mix}$ and the energetic part $\Delta \bar{U}_{mix}$:

$$\Delta \bar{S}_{mix} = -k \left[\frac{\phi_p}{N_p} \ln \phi_p + \frac{\phi_s}{N_s} \ln \phi_s \right]$$
$$\Delta \bar{U}_{mix} = \chi \phi (1 - \phi) kT$$

Together with the volume fraction $\phi = \phi_p = 1 - \phi_s$ and the definition for polymer solutions with a high molar mass polymer $N_p = N$ and a low molar mass solvent $N_s = 1$ this leads to the Flory Huggins equation [15]:

$$\Delta \bar{F}_{mix} = kT \left[\frac{\phi}{N} \ln \phi + (1 - \phi) \ln(1 - \phi) + \chi \phi (1 - \phi) \right] \tag{5}$$

The derivative of equation (5) by the number of solvent molecules n_s leads to its chemical potential difference $\Delta \mu_s$ between the solution and the pure solvent, which is also related to the osmotic pressure Π [22]:

$$\frac{\partial}{\partial n_s} \frac{\Delta \bar{F}_{mix}}{kT} = \frac{\Delta \mu_s}{kT} = -\frac{\Pi v_p}{kT} = \ln(1 - \phi) + (1 - \frac{1}{N})\phi + \chi \phi^2 \tag{6}$$

This osmotic pressure Π is a function of the vapor pressure of the solvent above the solution p and the vapor pressure of the pure solvent p_s like shown in equation (7). A detailed derivation can be found in [22].

$$-\frac{\Pi v_p}{kT} = \ln \left(\frac{p}{p_s} \right) \tag{7}$$

The polymer volume fraction is given by the reverse of relative film expansion $\phi = \frac{d_0}{d}$. This assumption is valid, because of the shape of the thin film. The lateral extent of the hydrogel is a few millimeter, whereas the film thickness is just a few hundred nanometer. Hence, an expansion of the film thickness is the main contribution to the volume change and the lateral expansion can be neglected. The molar mass N for a polymer is: $N \gg 1$. These considerations lead to the following equation (8).

$$\ln\left(\frac{p}{p_s}\right) = \ln\left(1 - \frac{d_0}{d}\right) + \frac{d_0}{d} + \chi\left(\frac{d_0}{d}\right)^2 \tag{8}$$

By inserting equation (2) the final equation is derived, that relates the change in thickness to RH:

$$RH = \left(1 - \frac{d_0}{d}\right) \exp\left(\frac{d_0}{d} + \chi\left(\frac{d_0}{d}\right)^2\right) \tag{9}$$

RH ... relative humidity; d_0 ... initial thickness of the hydrogel film; d ... actual thickness of the hydrogel film; χ ... Flory Huggins (interaction) parameter

Equation (9) directly relates the relative humidity RH to the thickness ratio, that is supposed to be measured. Since there are no further relations needed, the proposed approach to measure the RH value is a first principle measurement. A measurement system based on that principle could be even used without calibration. However, equation (9) contains the Flory Huggins parameter χ, which can display non-trivial dependences on composition, chain length and temperature. All deviations from the lattice model and all effects, that are not fully understood, are lumped into this parameter [15]. An analytic expression for equation (9) cannot be found. Hence, the Flory Huggins parameter χ must be empirically approximated for every hydrogel composition, by measuring the thickness change and the corresponding RH value simultaneously.

3.2 Humidity Generation

Humidity generation (also called humidification) refers to a process, that changes the total amount of water gas phase in the air. The application of Mollier h,x-diagrams is a common method to deal with such processes [23]. In the introduction it is already mentioned, that the relative humidity RH is a function of the temperature dependent equilibrium vapor pressure p_s of water (equation (2)). There exist several models for this temperature dependency. Equation (10) by Buck is the most accurate one [24] for the applied temperature range.

$$p_s = 611.21 \exp\left(\left(18.678 - \frac{T}{234.5}\right)\left(\frac{T}{257.14 + T}\right)\right) [Pa] \tag{10}$$

p_s ... equilibrium vapor pressure of water in Pa; T ... temperature in °C

With application of equation (10) together with equation (11) and (12), that are just rearranged versions from the equations in section 1.1, it is possible to calculate the water fraction x_1 in the actual air mixture, when the temperature and the RH value is known.

$$p = RH\ p_s \quad [Pa] \tag{11}$$

$$x = \frac{M_w}{M_a} \frac{p}{P - p} \quad \left[\frac{\text{g(water)}}{\text{g(air)}}\right] \tag{12}$$

x ... water fraction; M_w, M_a ... molecular weight of water, air; p ... partial pressure of water vapor; P ... total pressure

If the relative humidity of the ambient air (with known temperature and RH) should be increased to $100\,\%\mathrm{RH}$, the necessary water fraction x_2 can also be calculated with equations (10) - (12). The corresponding amount of water m_s, that must be evaporated, can be determined with equation (13).

$$x_2 = \frac{\overbrace{x_1 m_1 + m_s}^{\text{total mass of water}}}{\underbrace{m_1 + m_s}_{\text{total mass of humid air}}}$$

$$m_s = m_1 \frac{x_2 - x_1}{1 - x_2} \tag{13}$$

m_s ... mass of water that has to be evaporated; m_1 ... mass of ambient air that gets humidified; x_1, x_2 ... water fraction of the ambient air, and the humidified air (from equation (12))

The energy, that must be provided to evaporate that amount of water, can be calculated with equation (14). The quantities needed are the following: enthalpy of evaporation (at $100\,°\mathrm{C}$ and ambient pressure) $h_s = 2257\,\mathrm{kJ/kg}$; specific enthalpies for liquid water at ambient temperature $h_{w,20} = 83.9\,\mathrm{kJ/kg}$ and at $100\,°\mathrm{C}$ $h_{w,100} = 419.1\,\mathrm{kJ/kg}$ [25].

$$\Delta H = \left[h_s + (h_{w,100} - h_{w,20}) \right] m_s \tag{14}$$

3.3 Laser Interference

In general, interference is a phenomenon, which is the result of the superposition of two or more waves to form a resultant wave of lower, greater, or the same amplitude. Already more than 100 years ago, Charles Fabry and Alfred Perot suggested to use this phenomenon when „it is a question of measuring very small thicknesses or very small changes or differences in thickness" [26]. Based on these considerations, it is possible to find a model for measuring the absolute thickness of a thin film with a broadband light source and a spectrometer, correspondingly the relative change of thickness with a laser and a photodiode. Incident light at a multi-layered material is separated into reflected and transmitted parts. Reflection and transmission occurs at every interface, which is basically dependent on the difference of refractive indices and the incident angle, described by the so-called Fresnel equations. These equations follow from the solution of the wave equation within linear, isotropic media with plane waves. Together with the boundary conditions, that obey the laws of Electromagnetic Theory (the tangential component of the electric field must be equal on both sides of the interface), this yields to different equations for the reflection and transmission coefficient, depending on the polarization of the incident wave [27]. A corresponding schematic is sketched in figure 1.
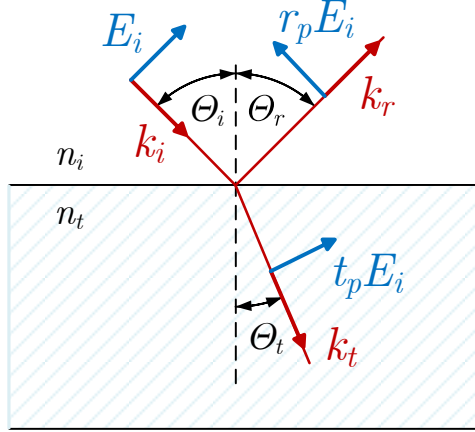
Figure 1: Schematic of the correlation between the reflection and transmission coefficients (r_p, t_p), according to Fresnel equations for p-polarized light; E_i is the electric field of the incident light; k is the propagation vector of the different light paths

Equation (15) and (16) apply for p-polarized light (where the electric field vector is parallel to the plane of incidence) at an interface between two dielectric materials, that have almost the same magnetic permeability. There are corresponding equations also for s-polarized light, where the electric field vector is perpendicular to the plane of incidence, but they are not relevant for this work.

$$r_p = \frac{n_t \cos(\theta_i) - n_i \cos(\theta_t)}{n_i \cos(\theta_t) + n_t \cos(\theta_i)} \tag{15}$$

$$t_p = \frac{2n_i \cos(\theta_i)}{n_i \cos(\theta_t) + n_t \cos(\theta_i)} \tag{16}$$

r_p, t_p ... (amplitude) reflection, transmission coefficient for incident p-polarized light; n_i, n_t ... refractive indices of the two media; θ_i, θ_t ... angles of the light path (also see figure 1)

If the behavior of an incident light beam on an interface is known, it is possible to set up the model for describing the interference phenomenon, that is expected. The sketch in figure 2 describes that model and helps to understand this effect.
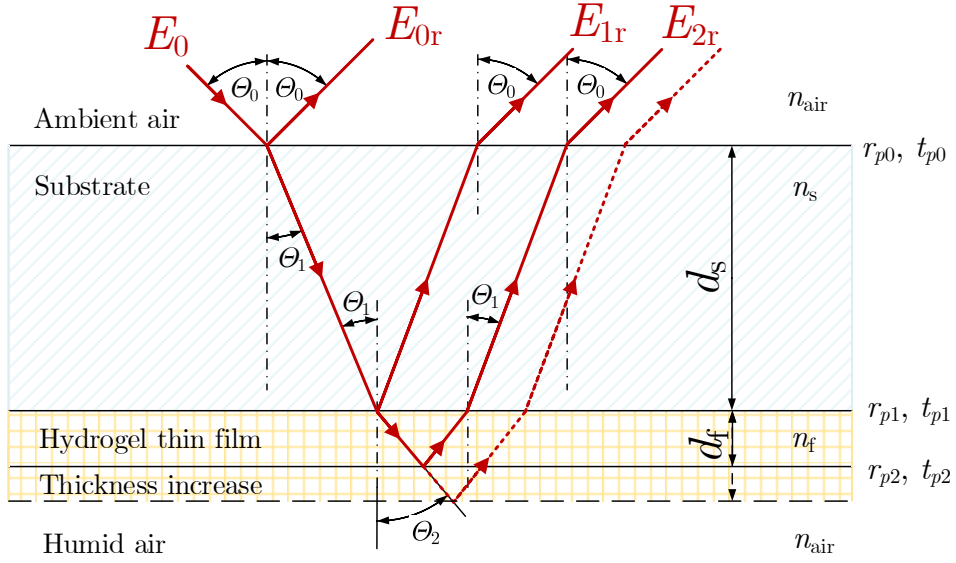
Figure 2: Sketch of the measurement principle for the thin film thickness on a substrate with different refractive indices (n_s, n_f). At every interface a light beam gets split up into a transmitted and reflected part, according to the coefficients (r_p, t_p) from Fresnel equations (15) and (16). Light that is transmitted at the initial interface and reflected later, travels an additional distance, which causes a phase shift (equation (23)). If the thickness increases, the path of E_{2r} gets elongated (dotted path) and the phase shift changes.

The quantity, that can be measured in optical experiments, is the intensity, which is basically the square of the electric field (equation (17)).

$$I_i = |E_0|^2 \tag{17}$$

with

$$E_0 = E_i e^{i(kz - \omega t)} \tag{18}$$

I_i ... intensity of the incident light; E_0 ... electric field of the incident light, E_i ... amplitude of the incident electric field

If you superimpose two or more electromagnetic fields, it is essential to sum up the electric fields before squaring the whole expression. This is the basis for all interference effects. The reflected intensity, that is expected to be measured, is shown in equation (19).

$$I_r = |E_{0r} + E_{1r} + E_{2r}|^2 \tag{19}$$

I_r ... intensity of the reflected light; E_{0r}, E_{1r}, E_{2r} ... reflected electric fields at the three interfaces according to figure 2

The model sketched in figure 2 is sufficient for components with a small difference in refractive indices and hence a small reflectivity. More electric field vectors have

to be taken into account in systems with higher reflectivity, because multiple reflections occur. The electric fields of equation (19) are mathematically described in equation (20) to (22). They consist of the incident field (equation (18)), multiplied with the corresponding reflection and transmission coefficients, based on the Fresnel equations (equation (15) and (16)) and an additional phase factor for the longer optical path, depending at which interface they got reflected. The general form for the phase factor δ is given by equation (23)

$$E_{0r} = r_{p0}E_0 = r_{p0}E_i e^{i(kz-\omega t)} \tag{20}$$

$$E_{1r} = r_{p1}t_{p0}^2 E_0 = r_{p1}t_{p0}^2 E_i e^{i(kz-\omega t+\delta_s)} \tag{21}$$

$$E_{2r} = r_{p2}t_{p0}^2 t_{p1}^2 E_0 = r_{p1}t_{p0}^2 t_{p1}^2 E_i e^{i(kz-\omega t+\delta_s+\delta_f)} \tag{22}$$

r_{pj}, t_{pj} ... (amplitude) reflection, transmission coefficients at the j-th interface; E_i ... amplitude of the incident electric field; k ... propagation vector of the incident light; z ... length of the light path, ω ... angular frequency of the light; t ... time; δ_f, δ_s ... additional phase factor of the reflected electric field, caused by the thin film and the substrate;

with

$$\delta = k\Lambda = \frac{2\pi}{\lambda}\Lambda \tag{23}$$

Λ ... optical path length difference; λ ... wavelength of the incident light

In figure 3 the optical paths of a two-beam reflection is depicted. For calculation of the optical path length difference Λ, a few geometrical considerations are necessary, which lead to equation (25).
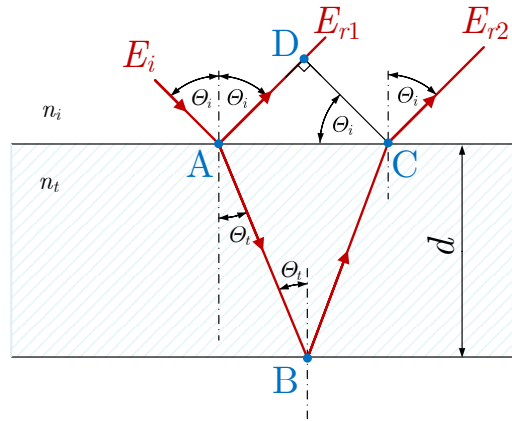

Figure 3: Detailed drawing of the light paths for two-beam reflection

$$\Lambda = \left(\overline{AB} + \overline{BC}\right)n_t - \overline{AD}n_i$$

$$\Lambda = 2\frac{d}{\cos\theta_t}n_t - \underbrace{2d\tan\theta_t}_{\overline{AC}}n_i\sin\theta_i$$

12

together with Snell's law $n_i \sin \theta_i = n_t \sin \theta_t$ [27]:

$$\Lambda = \frac{2n_t d}{\cos \theta_t} - 2n_i d \frac{\sin \theta_t}{\cos \theta_t} \frac{n_t}{n_i} \sin \theta_t = \frac{2n_t d}{\cos \theta_t} \underbrace{(1 - \sin^2 \theta_t)}_{\cos^2 \theta_t}$$

$$\Lambda = 2n_t d \cos \theta_t \tag{24}$$

or in terms of the incident angle θ_i:

$$\Lambda = 2n_t d \sqrt{1 - \sin^2 \theta_t} = 2n_t d \sqrt{1 - \frac{n_i^2}{n_t^2} \sin^2 \theta_i}$$

$$\Lambda = 2d \sqrt{n_t^2 - n_i^2 \sin^2 \theta_i} \tag{25}$$

For a mathematical description of the interference effect, it is necessary to perform the calculation in equation (19). Due to physical reasons (the incident angle is not exceeding the angle of total reflection), the coefficients can be defined as $r_p, t_p \in \mathbb{R}$:

$$I_r = |E_{0r} + E_{1r} + E_{2r}|^2 = (E_{0r}^* + E_{1r}^* + E_{2r}^*)(E_{0r} + E_{1r} + E_{2r})$$

$$I_r = \underbrace{E_{1r}^* E_{2r} + E_{2r}^* E_{1r}}_{I_{12}} + \underbrace{E_{0r}^* E_{2r} + E_{2r}^* E_{0r}}_{I_{02}} + \text{constant terms}$$

$$I_r = I_{12} + I_{02} + \text{constant terms} \tag{26}$$

with the two interference terms I_{12} and I_{02}

$$I_{12} = r_{p1} t_{p0}^2 r_{p2} t_{p0}^2 t_{p1}^2 E_i^2 \left(e^{-i(kz - \omega t + \delta_s)} e^{i(kz - \omega t + \delta_s + \delta_f)} + e^{i(kz - \omega t + \delta_s)} e^{-i(kz - \omega t + \delta_s + \delta_f)} \right)$$

$$I_{12} = r_{p1} r_{p2} t_{p0}^4 t_{p1}^2 E_i^2 \left(e^{-i\delta_f} + e^{i\delta_f} \right)$$

$$I_{12} = 2R_{12} T_0^2 T_1 E_i^2 \cos \delta_f \tag{27}$$

$$I_{02} = r_{p0} r_{p2} t_{p0}^2 t_{p1}^2 E_i^2 \left(e^{-i(kz - \omega t)} e^{i(kz - \omega t + \delta_s + \delta_f)} + e^{i(kz - \omega t)} e^{-i(kz - \omega t + \delta_s + \delta_f)} \right)$$

$$I_{02} = r_{p0} r_{p2} t_{p0}^2 t_{p1}^2 E_i^2 \left(e^{-i(\delta_f + \delta_s)} + e^{i(\delta_f + \delta_s)} \right)$$

$$I_{02} = 2R_{02} T_0 T_1 E_i^2 \cos(\delta_f + \delta_s) \tag{28}$$

R_j, T_j ... Reflectance, transmittance at the j-th interface; E_i ... amplitude of the incident electric field; δ_f, δ_s ... additional phase factor of the reflected electric field, caused by the thin film, and the substrate;

The film thickness dependency is contained in the phase factor δ_f (equation (29)) of the interference term I_{12}. All the other components in the exponent cancel each other.

$$\delta_f = \frac{4\pi}{\lambda} d_f \sqrt{n_f^2 - n_s^2 \sin^2 \theta_0} \tag{29}$$

$$\delta_s = \frac{4\pi}{\lambda} d_s \sqrt{n_s^2 - n_{air}^2 \sin^2 \theta_0} \tag{30}$$

λ ... wavelength of the incident light; d_f, d_s ... thickness of the thin film and the substrate; n_f, n_s, n_{air} ... refractive index of the thin film, substrate and air; θ_0 ... incident angle

In fact, there is a second interference term I_{02} (equation (28)), that contains not just the film thickness d_f, but also the thickness of the substrate d_s. This issue has to be overcome, because already small deviations of the nominal thickness of the substrate generate an unknown phase shift. A thickness measurement with an accuracy of a few nanometers would be necessary to determine the correct phase shift. This is simply not possible for a substrate with a thickness of a few millimeters.

Both interference terms consist of a cosine function and some multiplicative pre-factors. By comparison of the two terms it can be seen, that just I_{02} contains the reflectance term $R_{02} = r_{p0}r_{p2}$. In fact, I_{02} can be minimized by minimizing r_{p0}. Due to some preparatory work, the refractive index of pHEMA is known and lies around 1.5. The reflection coefficients are maximized by using a substrate material with a considerably higher refractive index compared to the hydrogel. Sapphire ($n_s = 1.7659$) is a possible choice for the substrate. Figure 4 shows the result of the Fresnel equation for the reflection coefficient of p-polarized light r_p as a function of the incident angle θ_0 (equation (15)) for the three interfaces shown in figure 2. The applied refractive indices are $n_{air} = 1.0003, n_s = 1.7659, n_f = 1.514$.
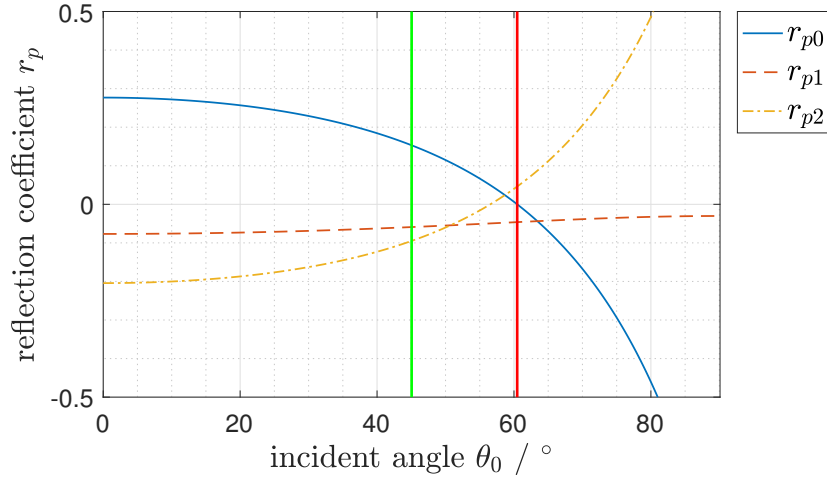

Figure 4: Result of the Fresnel equation for the reflection coefficient of p-polarized light r_p as a function of the incident angle θ_0 (equation (15)) for the three interfaces $(0, 1, 2)$ shown in figure 2 ($n_{air} = 1.0003; n_s = 1.7659; n_f = 1.514$). The solid red line marks the Brewster angle (r_{p0} gets zero) and the solid green line another incident angle at $45.05°$

Evidently, the reflection coefficient at the initial interface r_{p0} becomes zero at the Brewster angle. Performing the measurements at this incident angle should minimize I_{02} or ideally neglect it completely. In the following plots the reflected intensity is divided by $I_i = E_i^2$. This cancels the factor E_i^2 in I_r and thus the remaining expression is independent of the incident intensity.

Figure 5 shows the computed reflection factor (equation (26) divided by I_i) as a function of the film thickness for the Brewster angle as the incident angle θ_0. At a first sight, it seems to be difficult to refer to a unique thickness value by measuring the reflection, because there are more solutions possible at a certain intensity value. Considering an initial thickness of $400\,\text{nm}$ and assuming a thickness increase

of about 30 % (which is realistic for pure pHEMA according to [13]), this would cause a decrease in intensity just between the maximum at about 390 nm and the minimum at 510 nm. With this interference model and a known initial thickness, a measurement of the difference in reflected intensity is sufficient to refer to a relative change in thickness. That is necessary for equation (9) and leads to a RH value in the end. Figure 6 shows the theoretic interference pattern for an incident angle θ_0 of 45.05° and hence the influence of a non-zero reflection coefficient r_{p0} at the initial interface. Compared to figure 5 it is shifted and compressed.
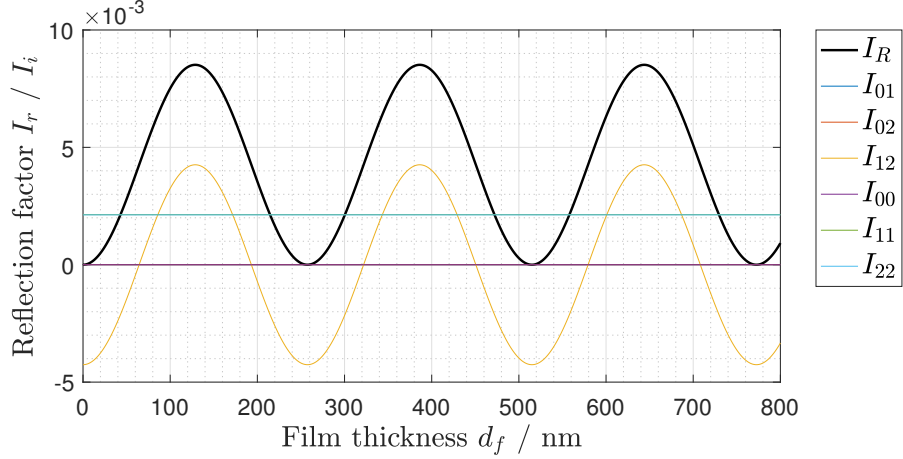

Figure 5: Theoretic interference pattern (equation (19)) at the Brewster angle as incident angle. The black curve is the sum of all other curves. In this case all terms that are dependent on the reflection at the initial interface (0) are zero. Just I_{12}, I_{22} and I_{11} (very low) contribute.
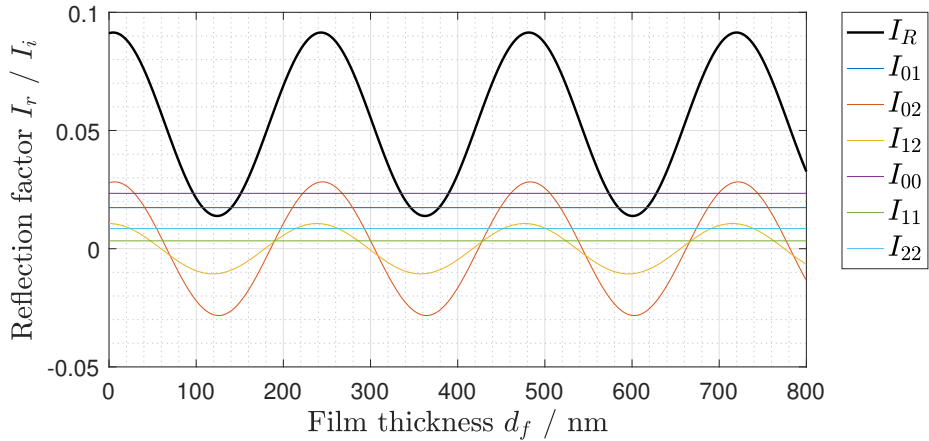

Figure 6: Theoretic interference pattern (equation (19)) for an incident angle θ_0 of 45.05°. The black curve is the sum of all other curves. In this case all terms contribute. Due to the fact that I_{02} is not negligible a phase shift compared to figure 5 can be observed

That specific incident angle is chosen, in order to demonstrate a case, where the interference pattern is shifted approximately one half cycle at an initial thickness of 400 nm. An increase of this thickness would yield to an increase of intensity.

Obviously, the interference pattern changes, because by tilting the sample, the path lengths of the light get modified. Another problem is the dependency of the phases shift on the thickness of the substrate. Already a deviation of about $0.6\,\mu m$ from the nominal value would cause a shift of a whole period. For mechanical stability, the substrate has at least to be around $1\,mm$ thick. So, the allowed uncertainty would be far less than $0.06\,\%$, which is not realistic due to practical reasons. Otherwise a calibration measurement for every substrate would be needed. A second disadvantage is the enormous sensitivity to angular changes and thus also to vibrations in the measurement setup. Assuming again a substrate thickness of about $1\,mm$, already a difference of $0.01°$ would cause a shift from a maximum to a minimum at a certain thickness value. Hence, angular changes in the order of $0.001°$ would influence the measured signal already significantly.

According to the issues stated above, it is decided to perform the measurements at the Brewster angle as the initial angle.

3.4 White Light Interference (Spectral Reflectance)

Regarding the Flory-Huggins model (equation (9)), it is sufficient to measure just a relative change in thickness to derive a RH value. A possible way of measuring it is described in section 3.3. For the application of this method, it is necessary to know the initial thickness of the hydrogel thin film. This can be achieved by measuring the reflected spectrum of an incident broadband light beam. The model function (equation (19)) is basically the same like for the laser interference described in section 3.3. The only difference is the reflection at the initial interface, that is not part of the interference model. For interference phenomena, the coherence length of the light source is a crucial factor. Reflected light beams can just interfere with each other, if the path difference is lower than the coherence length [28]. Light from diode lasers exhibits a coherence length of about $1\,m$ and more, whereas broadband light sources like halogen lamps lie around 10 to $100\,\mu m$ [29]. Substrates are much thicker than $100\,\mu m$ due to mechanical stability. So the interference term I_{02} of equation (26) vanishes. Together with equation (27) and (29) this leads to the following equation (31).

$$I_r = I_{12} + \text{constant terms}$$

$$I_r = 2R_{12}T_0^2 T_1 E_i^2 \cos\left(\frac{4\pi}{\lambda}d_f\sqrt{n_f^2 - n_s^2 \sin^2\theta_0}\right) + \text{constant terms} \qquad (31)$$

R_j, T_j ... Reflectance, transmittance at the j-th interface; E_i ... amplitude of the incident electric field; λ ... wavelength of the incident light; d_f ... thickness of the thin film; n_f, n_s ... refractive index of the thin film and substrate; θ_0 ... incident angle

In contrast to the film thickness dependent plots in section 3.3, figure 7 shows the reflection factor (equation (31) divided by I_i) over the wavelength. The model leads to a unique interference pattern for every thickness value of the thin film. By a fit of recorded spectral data, the absolute thickness of the thin film can be derived.
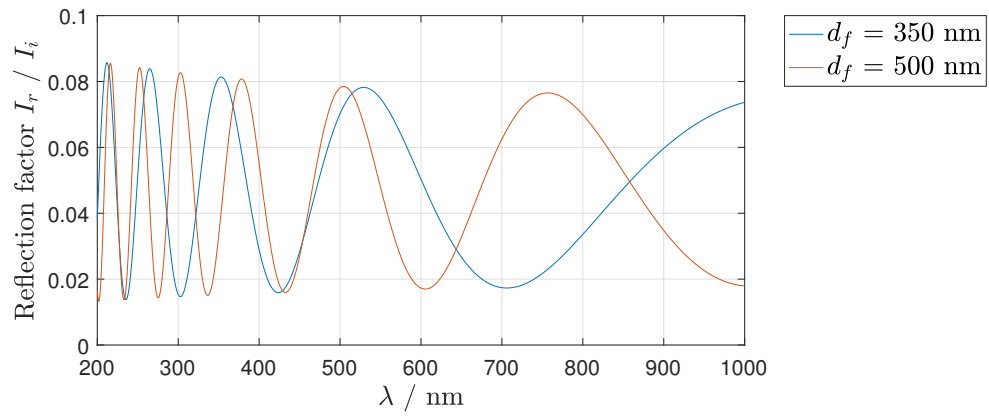
Figure 7: Theoretic spectral reflectance interference pattern for two different thicknesses of the hydrogel thin film: blue for $350\,\mathrm{nm}$ and red for $500\,\mathrm{nm}$

4 Experimental Setup

The experimental realization can be divided into several parts. As already mentioned in section 2.1, finding an appropriate material composition and deposition of the thin film on the substrate is the task of a second thesis. The actual thin film deposition is performed by *Sebastian Peterka*, who works on this thesis. The focus in this work is on the controlled generation of humidity and the optical measurement of the thickness change of the hydrogel thin film.

4.1 Deposition of the Hydrogel Thin Film

For the evaluation of a thickness measurement system, it is advantageous if the thickness change is sufficiently high. According to previous work, an appropriate swelling behavior can be expected from pure pHEMA without addition of EGDMA [13]. It also shows, that pure pHEMA is water soluble, which might sound unfavorable at first sight. However, it has a practical advantage, that thin film layers, which get destroyed by any cause, can be removed easily with just water and deposited again. Also different layer thicknesses can be produced with the same substrate by simply removing the previous one. The deposition is performed with an established reactor in a so called initiated chemical vapor deposition (iCVD) process. The method is based on a radical polymerization, in which free radicals react with non-radical monomers to form long polymer chains. Ideally, at the relatively mild conditions, that are required to decompose the initiator, the monomers retain their organic functionality [30].

An in-situ control of the exact layer thickness on the sapphire substrate can not be performed with this setup. Nevertheless, the layer thickness can be controlled indirectly with a laser interference setup, that monitors the layer thickness on an additionally placed piece of a silicon wafer in the reactor. Unfortunately, different substrates show different deposition rates and therefore the thickness on the silicon is not the same as on the sapphire substrate. Furthermore, the deposition process cannot be stopped abruptly. Hence, the layer thickness on the substrate can be controlled rather inaccurately. This is acceptable for a proof of concept. However, this would be a problem for an industrial product, because the reflected laser intensity changes with the initial layer thickness.

After the deposition, the thickness and optical properties are measured with an ellipsometer (J.A. Woollam Co. Inc.; M-2000V). The results are listed in table 3 and table 4. The refractive index for transparent thin films can be modeled by the Cauchy relationship shown in equation (32) [31].

$$n(\lambda) = A + \frac{B}{\lambda^2} + \frac{C}{\lambda^4} \tag{32}$$

$n(\lambda)$ ... wavelength dependent refractive index; λ ... wavelength; A, B and C ... fit parameters

Ellipsometer measurements are based on modeling the layer structure of the thin film and the substrate. The more one knows about the sample, the better the results get. Measurements with silicon substrates are well-established and therefore

resolutions of sub-nanometer are possible. Unfortunately, a transparent substrate complicates the measurement process due to back reflection and and leads to rather high uncertainties.

4.2 Humidity Generation

In general, accurate and stable humidification is a challenging task. Even expensive, commercial systems, that are based on the NIST proven *Two Pressure* principle, just offer a range of 5.2 to 99 %RH [32].

Together with the considerations in section 3.2 and the input parameters listed in table 1, the requirements for the evaporator could be set.

Table 1: Boundary conditions for the determination of the water evaporation rate

Property	Value
Ambient temperature T	24 °C
Ambient relative humidity RH	40 %RH
Ambient pressure P	1013.25 hPa
Target flow rate air m_1	25 L/min

The target air flow rate is converted to g/min with the density for ambient air $\rho_{air} = 1.19\,\text{g/L}$ derived with the ideal gas law and the specific gas constant for air $R_{air} = 287.1\,\text{J/(kgK)}$ [25].

The resulting water flow rate, that must be evaporated, is according to equation (13) $m_s = 20.8\,\text{g/h}$. Inserting of a flow rate in equation (14) leads to a power rather than an energy. The power needed for the evaporation of the calculated water flow rate is $P = 17.4\,\text{W}$. These are the minimum requirements for the evaporator to fulfill.

The implementation was realized with components, that were already available at the *Institute of Electronic Sensor Systems* for other projects. The used evaporator provides a range for the evaporation rate from 25 g/h to 1000 g/h, which seems a bit overpowered. However, the final setup, described in the following section is designed in a way, that the air gets over-saturated anyway and the excess water condenses in the separator after the cooling.

A schematic of the setup is drawn in figure 8 and the devices used for it are listed below:

Direct evaporator *aSTEAM* DV-4 series; evaporation rate: 25 g/h - 1000 g/h
      Manufacturer: aDROP Feuchtemeßtechnik GmbH
      Item no.: ATHMOS/MK/T–1502–1

Dosing pump for fluids; pumping speed: 1-100 mL/min
      Manufacturer: KNF Neuberger GmbH
      Item no.: Simdos 10

Mass flow controler red-y smart series; max. standard flow rate: 25 L/min air
  Manufacturer: Vögtlin Instruments GmbH
  Item no.: GSC-C9TA-BB12

Vacuum pump oil-free; inlet capacity: $25 \, m^3/h$
  Manufacturer: Becker GmbH
  Item no.: WB 63 A2 STP

According to the objective stated in section 2.1, some requirements to the system are defined. All measurements are performed at constant room temperature and the required dynamic range is defined from 10 to 95 %RH. As already mentioned in section 1.1, the definition of RH implies temperature dependency. Instead of adding an additional control parameter, the setup is realized in a way, that the humid air outlet stays sufficiently constant at the same temperature as the ambient air. Since the Flory-Huggins interaction parameter is also temperature dependent, this is an important demand. An investigation of its temperature dependency would be interesting, but is omitted, in order to simplify the generator setup. However, an implementation in the future would be still possible with the actual setup.

The flow rate of the humid air is set to 25 L/min, due to the limitations of the available mass flow controller. By keeping the volume of the measurement chamber low, the rate should be high enough to exchange the air in the whole chamber sufficiently fast and get short response times for variation of RH.
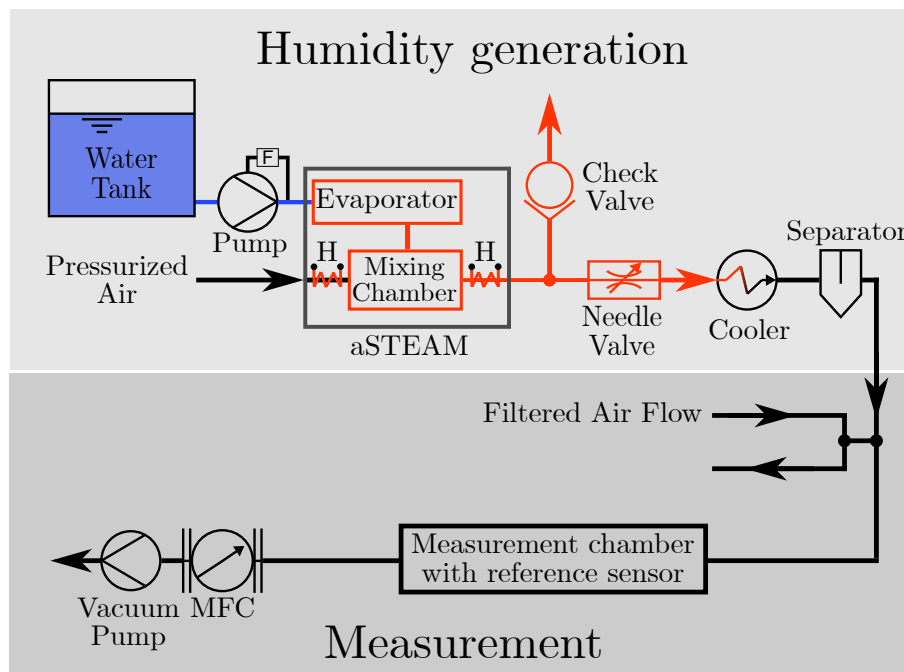

Figure 8: Schematic of the humidity generation setup.

The core component of the setup is the *aSTEAM* direct evaporator. These evaporators have the advantage, that no carrier gas is needed like for bubbler systems. All the delivered liquid gets entirely evaporated. This is realized by spraying the liquid in the evaporation chamber in a way, that it gets highly dispersed. The necessary energy for evaporation is generated by electrical heating elements. The electrical power of the heater is automatically adjusted to the quantity of the liquid, that is

delivered by the pump. With a water pump, that stably delivers a certain amount water, an entire and pulsation free evaporation is possible [33]. The used direct evaporator does not just provide an evaporation stage, but also a heated mixing chamber, where the steam can be mixed with different kinds of preheated gases. Pressurized air is used in the actual setup. Due to preheating, condensation at that stage is avoided.

After the mixing chamber, the air mixture is saturated and has a temperature of about $100\,°C$. The exact RH value is not that important at that point, because it gets cooled down anyway. If the following needle valve is closed completely, the entire air mixture is released to atmosphere through an attached check valve. Owing to rather high temperatures, PTFE tubes are used for the connection of the components. The cooler consists also of a PTFE tube in ambient atmosphere, that is sufficiently long to cool down the humid air. By cooling a humid gas mixture, the equilibrium vapor pressure is decreased, whereas the partial pressure of water stays the same. Condensation occurs, when the equilibrium vapor pressure drops below the actual partial pressure of water. Therefore, a liquid water separator is placed after the cooler, which is a bottle with an inlet and an outlet in the cap. The condensed water is collected at its bottom. After the separator, the humid air is in a condition with theoretically $100\,\%RH$ at room temperature.

At the end of the setup, a vacuum pump is placed together with a mass flow controller (MFC). If the needle valve is entirely closed, it draws just filtered air, that moderately flows by the system through a H-connector, attached before the measurement chamber. By turning up the needle valve, the amount of humid air is increased. The pump then draws a mixture of filtered and humid air. With the opening position of the needle valve, the mixing ratio and hence the RH value of the air in the measurement chamber can be controlled.

A dynamic humidity range of $3\,\%RH$ to $97\,\%RH$ could be achieved with the described setup, measured by the reference sensor. The stability of the RH setting is sufficient within $\pm2\,\%RH$. This fluctuation is due to a periodical release of the steam at the check valve. Obviously, pressure needs to be built up to overcome the spring of the valve. At high RH levels ($> 85\,\%RH$), the humidity setting starts to drift slightly, but can be easily compensated manually. The residual humidity of the filtered air marks the baseline of the adjustable RH range. If the needle valve is fully open, the humid air does not get entirely cooled down and therefore condensation at the walls of the chamber can occur. This could damage the thin film layer as well as the reference sensor and is avoided at any costs. However, generation of even higher humidity levels would be possible, but was not performed.
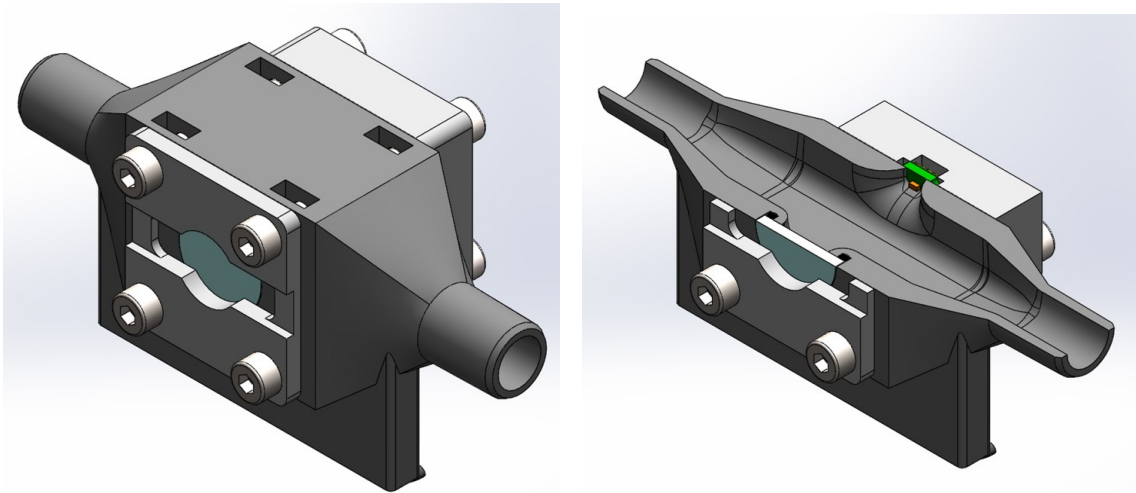
4.3 Humidity Measurement

The humidity measurement setup is based on the thickness change of a hydrogel thin film, like explained in section 3.3. It is implemented on an Aluminum breadboard to facilitate transportation. Furthermore, a commercial humidity reference sensor is implemented for evaluation and calibration of the system.

4.3.1 Laser Setup

As defined in section 2.2, the thickness should be measured from the backside of the substrate. A 3D model of the measurement chamber, that fulfills the demands, is depicted in figure 9. The modeled chamber is printed with a stereo lithographic 3D printer (Formlabs Form 2). The substrate is a Ø17.25 mm sapphire glass window, with the thin film deposited on the surface facing the inside volume of the chamber. Sapphire is used, because its refractive index is considerably higher ($n_s = 1.7659$) than pHEMA, which is about 1.51, according to previous measurements and is still affordable. A normal glass window like BK-7 cannot be used, because its refractive index is similar to pHEMA and therefore the reflection would be weaker.

The reference sensor is placed exactly on the opposite side of the sapphire window to ensure, that a sudden change of humidity in the air flow affects both at the same time. The chamber is designed symmetrically with connectors for a hose on both sides. The humid air is drawn straight through the chamber by the vacuum pump, that is connected to one side. The chamber is sealed with an O-ring at the window and with PTFE tape at the reference sensor side. Both parts are mounted exchangeably with adapters and screws. The chamber itself is designed in a way, that sharp edges are avoided in the gas flow. Just in case that condensation occurs, there are no parts mounted at the bottom of the chamber.

(a) Full 3D model

(b) Cross section of the 3D model

Figure 9: Measurement chamber for the optical setup. The sapphire window coated with the hydrogel is colored in light blue and the reference sensor on the back side in green. The cylindrical shaped connectors on the left and right side are implemented for attaching the hose of the humidity generator and the vacuum pump on either side.

The measurement chamber is mounted on a precision rotation stage to adjust the Brewster angle properly and minimize the reflection at the initial interface. The whole setup is shown in figure 10. A diode laser is used as the light source. The incident light gets p-polarized with a linear polarizer. The iris diaphragm is used for limiting the lateral extend of the light beam, in order to irradiate the sapphire window just in its center, which is in contact with the humid air. The reflected light

goes through a rotatable linear polarizer and is detected with a power meter, where a laser line filter is mounted to eliminate any unwanted stray light.
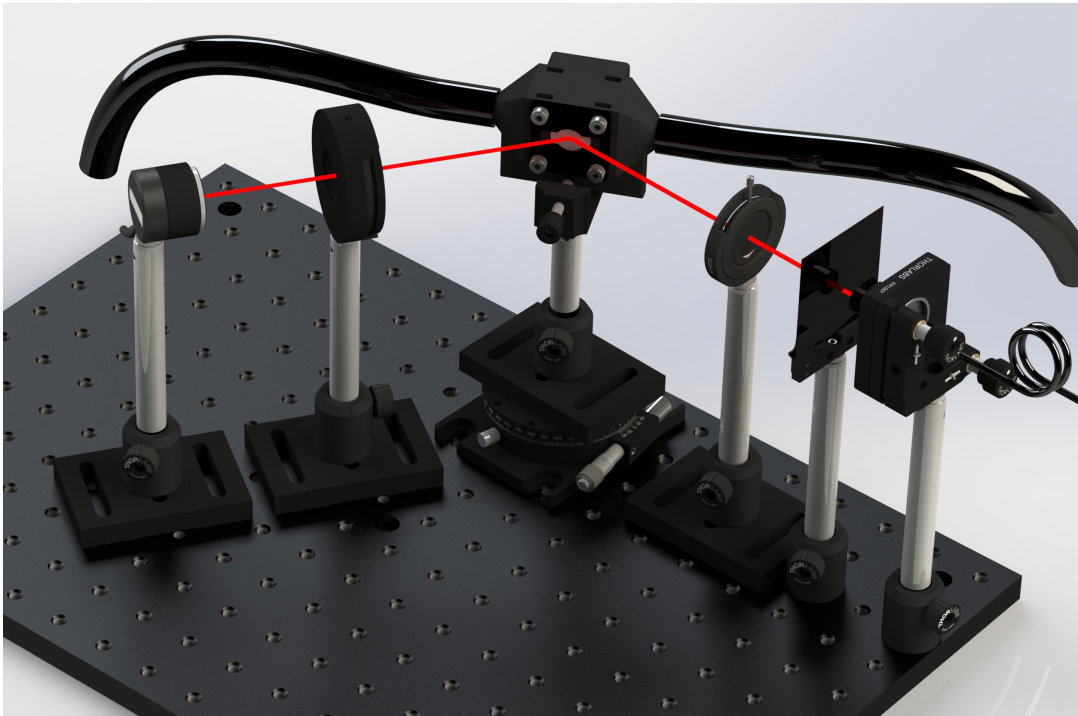

Figure 10: 3D rendered model of the optical thin film measurement setup. The measurement chamber is mounted on top of a precision rotation stage. The incident path is realized with a laser diode, a linear polarizer and an iris diaphragm. The reflection path contains a rotatable linear polarizer and a detector with attached laser line filter.

The following components are used for the laser interference optical setup:

Laser Diode Center wavelength: 638.7 nm (according to specification sheet); Output power: 4.6 mW; Elliptical beam; Power stability 2 %
Manufacturer: Thorlabs Inc.
Item no.: CPS635

Linear Polarizer $2''$ x $2''$ polarizer sheet
Manufacturer: Thorlabs Inc.
Item no.: LPVISE2X2

Iris Diaphragm 12 mm max aperture
Manufacturer: Thorlabs Inc.
Item no.: ID12/M

Rotation Mount High-precision; Micrometer: 2.4 arcmin rotation per division
Manufacturer: Thorlabs Inc.
Item no.: PR01/M

Sapphire Window Al_2O_3; Uncoated; Ø17.25x2 mm,
Manufacturer: Edmund Optics Ltd.
Item no.: #43-633

Linear Polarizer with rotation mount for Ø1″ optics
        Manufacturer: Thorlabs Inc.
        Item no.: LPVISE100-A with RSP1D/M

Laser Line Filter Center wavelength: $(635 \pm 2)\,\text{nm}$; FWHM: $(10 \pm 2)\,\text{nm}$
        Manufacturer: Thorlabs Inc.
        Item no.: FL635-10

Photodiode Power sensor; Si; Wavelength range: $400\,\text{nm}$ - $1100\,\text{nm}$; Power range:
        $50\,\text{nW}$ - $50\,\text{mW}$; Uncertainty: $\pm 3\,\%$ (betweeen 440 - $980\,\text{nm}$)
        Manufacturer: Thorlabs Inc.
        Item no.: S120C

USB Power and Energy Meter Interface for C-type sensors
        Manufacturer: Thorlabs Inc.
        Item no.: PM100USB

Aluminum Breadboard $300\,\text{mm}$ x $450\,\text{mm}$ x $12.7\,\text{mm}$
        Manufacturer: Thorlabs Inc.
        Item no.: MB3045/M

Various Mounts Posts, post holders and mounting plates
        Manufacturer: Thorlabs Inc.
        Item no.: -

In order to compare the measured results with actual RH values, the following reference sensor is used:

Digital Humidity Sensor Specified range: 0-100 %RH, Uncertainty: $\pm 2\,\%$ (95 %
        confidence interval [34]); Response time $\tau_{63} < 8\,\text{s}$, with USB Evaluation Kit
        Manufacturer: Sensirion AG
        Item no.: SHT31 with EK-H5

4.3.2 Extended Setup

Even if the white light inference setup is just necessary for an initial measurement, the design of the principle setup provides the opportunity to implement and evaluate both described thickness measurement methods (section 3.3 and 3.4) simultaneously. This gives the possibility to verify the results from the laser interference with a second method. The setup is shown in figure 11. The fiber decoupler and coupler for the white light interference setup are realized with bi-convex lenses and are placed in the space between incident and reflected beam. An iris diaphragm spatially constraints the light spot coming from the tungsten halogen light source on the sapphire window. The reflected beam gets coupled into a fiber, that is attached to the spectrometer. Except of a small amount of stray light, the light path does not interfere with the laser beam, because the incident and reflection angles are different.

For the white light interference extension of the setup, the following components are used:

Tungsten Halogen Light Source for the Vis-NIR (360 nm - 1700 nm); Output
power: 7 W; Power stability: 0.5 %
Manufacturer: Ocean Optics Inc.
Item no.: HL-2000-HP-FHSA, Serial no.: 034990880

Modular Spectrometer Flame series; Grating: 500 line/mm blazed at 250 nm;
Bandwidth: 200 nm - 1027 nm; Resolution: 1.2 nm FWHM
Manufacturer: Ocean Optics Inc.
Item no.: FLMS03847

Fibers Core diameter: 600 µm; Bandwidth: 200 nm - 1100 nm
Manufacturer: Ocean Optics Inc.
Item no.: P600-1-SR and QP600-2-SR-BX

Bi-convex Lenses N-BK7; Uncoated; f = 50 mm and f = 60 mm
Manufacturer: Thorlabs Inc.
Item no.: LB1471 and LB1596

Iris Diaphragm 25 mm max aperture
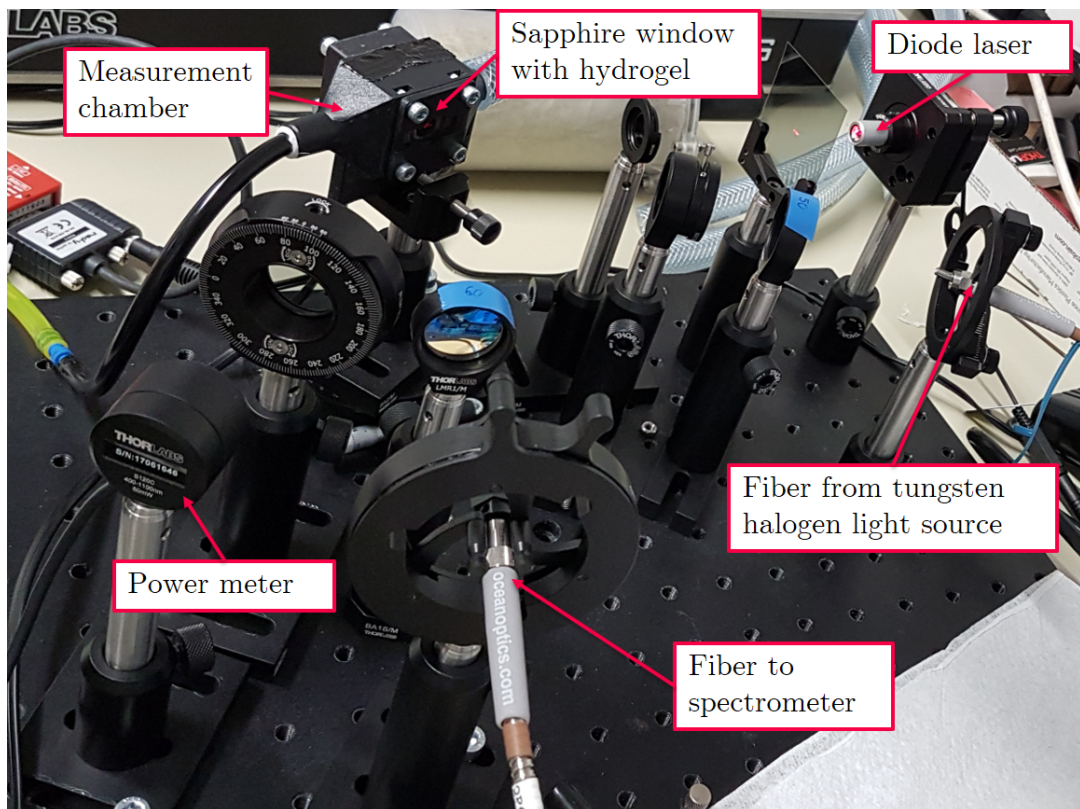Manufacturer: Thorlabs Inc.
Item no.: ID25/M

Figure 11: Picture taken from the extended setup with the fiber, that couples in the light from the tungsten halogen light source and the one, that is attached to the spectrometer.

4.3.3 Fiber Version

If the hydrogel thin film is deposited directly onto the tip of a fiber, this initial interface between air and the backside of the substrate can be avoided. Hence, all considerations in section 3.3 about performing the measurements at the Brewster angle are expendable with this strategy. Furthermore there are just a few components needed and no alignment must be performed, which makes the implementation quite simple. An application of both measurement principles (laser or white light interference) is possible with this setup. A picture of the setup in white light interference configuration is shown in figure 12.

The components needed for this setup are the following:

Tungsten Halogen Light Source for the Vis-NIR (360 nm - 1700 nm); Output power: 7 W; Power stability: 0.5 %
Manufacturer: Ocean Optics Inc.
Item no.: HL-2000-HP-FHSA, Serial no.: 034990880

Modular Spectrometer Flame series; Grating: 500 line/mm blazed at 250 nm; Bandwidth: 200 nm - 1027 nm; Resolution: 1.2 nm FWHM
Manufacturer: Ocean Optics Inc.
Item no.: FLMS03847

Fiber beam splitter Core diameter: 400 µm; Bandwidth: 300 nm - 1100 nm
Manufacturer: Ocean Optics Inc.
Item no.: SPLIT400-UV-VIS

An implementation for a laser interference measurement would be possible, if the light source is replace by a laser and the spectrometer by a photodiode.

The main part is a fiber beam splitter with the hydrogel thin film deposited directly onto the tip of the single leg. The light source is attached to one leg of the fiber beam splitter. The light gets transmitted through the beam splitter to the tip, where the hydrogel thin film is deposited. A fraction of the light gets reflected at the first interface between the glass core and the hydrogel. Reflection occurs also at the second interface between the hydrogel and the ambient air. Light from these two reflections interferes with each other in the same way as explained in section 3.3. The reflected light gets transmitted backwards to the beam splitter. According to the splitting ratio of the fiber (which is 50:50), the reflected light gets split into the two legs. The detector (spectrometer or power meter) is attached to the second leg and records the light coming from the beam splitter. The evaluation of the detected signal is the same as for the other setups, just with an incident angle of 0°.
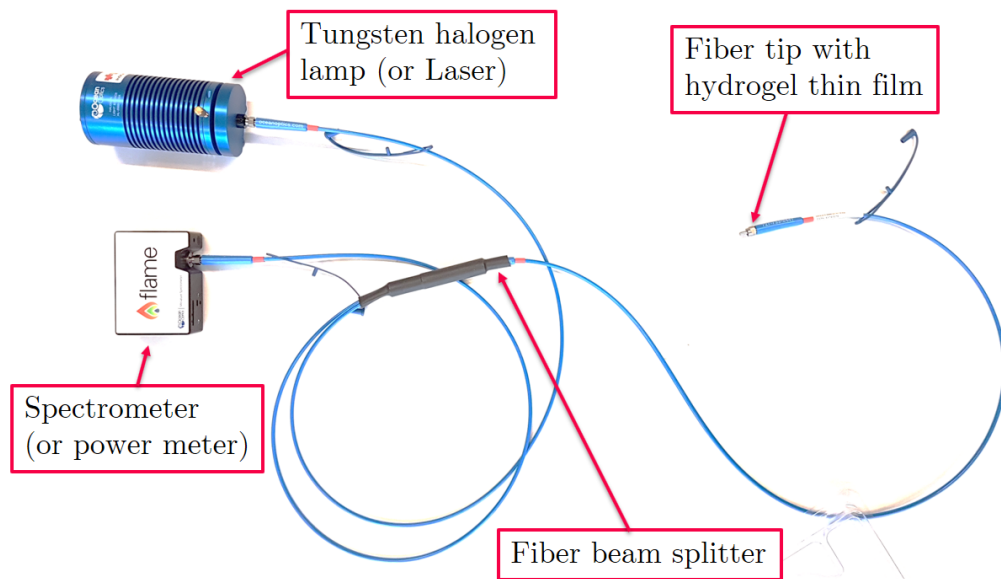
Figure 12: Measurement setup with the fiber beam splitter in a white light interference configuration. With the application of a laser instead of the tungsten halogen lamp and a power meter instead of the spectrometer, a laser interference measurement can also be performed.

5 Measurements and Results

The measurements are performed with the setup described in the previous sections and the parameters listed in table 2. These are found by several measurements, in order to optimize the humidity generation and measurement process. Unless declared differently, the parameters are the same for all measurements. Two different depositions are used to investigate the proposed measurement principles. The second deposition was necessary because the extended setup did not lead to reproducible results with the first one.

Table 2: General parameters for the humidity measurements shown in section 5.1 and 5.2

Instrument	Parameter	Value
Vacuum pump	Pumping speed	25 L/min
Water pump	Pumping speed	10 mL/min
Manometer air inlet aSTEAM	Pressure	2 bar
aSTEAM evaporation stage	Temperature	120 °C
aSTEAM mixing chamber	Temperature	100 °C
Manometer filtered air flow	Pressure	<1 bar
Power Meter	Integration time	1 s
Humidity reference sensor	Integration time	1 s

5.1 Deposition Sample No. 1

The measurements described in this subsection are performed with a sapphire window, that got coated on the 12.07.2017. After the deposition, the thickness and optical properties of the thin film layer are measured with the ellipsometer, which are listed in table 3. The measurement is performed at ambient conditions. The value for the thickness is just a rough estimate at unknown RH, because it changes according to the surrounding humidity level of course. As already mentioned in section 4.1, just pure pHEMA is used due to practical reasons. Most of the measurements are performed at an initial angle of 60.5°, according to the considerations described in section 3.3.

Table 3: Composition, thickness and optical parameters for the refractive index (equation (32)) of deposition sample no. 1 performed on the 12.07.2017

Property	Value
Amount of HEMA	100 %
Amount of EGDMA	0 %
Layer thickness	(695 ± 17) nm
Parameter A	1.59 ± 0.03
Parameter B	0.0037 ± 0.0008
Parameter C	0

For the evaluation of the coated sapphire window and the measurement setup, various humidity settings are applied to the system. This is done by changing the opening position of the needle valve, which is described in section 4.2. The reflected laser power and the reference RH value are recorded over time with the power meter and the humidity reference sensor. In order to show the influence, measurements at two different incident angles are performed with the same sapphire window (figure 13 and 15).

Interesting features are depicted in figure 13 for a measurement at an incident angle of 60.5°, which is the Brewster angle for the actual material configuration. It shows the measured power of the reflected laser light, captured with the power meter (left axis - blue curve) and the RH value, measured with the reference humidity sensor (right axis - red curve). A non-linear correlation between those two signals can be clearly observed. Apparently, the signal increase at high RH values is much bigger than for low RH values. Furthermore, an increase of RH leads also to an increase of the reflected power. According to the theoretic model plotted in figure 5 and the measured thickness of $(695 \pm 17)\,\mathrm{nm}$, the signal should decrease in that regime. So, the model is contrary to the results and needs further investigation.
The inertia of the reference humidity sensor with respect to the reflected power signal is a prominent feature, especially at the signal drop at about 330 s. While the blue curve reaches its bottom value quite abruptly, it takes much longer for the red curve. The same effect also occurs at the signal increase, but is harder to investigate in figure 13 due to the non-linearity of the signal correlation. A detailed discussion of the phenomenon can be found in section 6.2
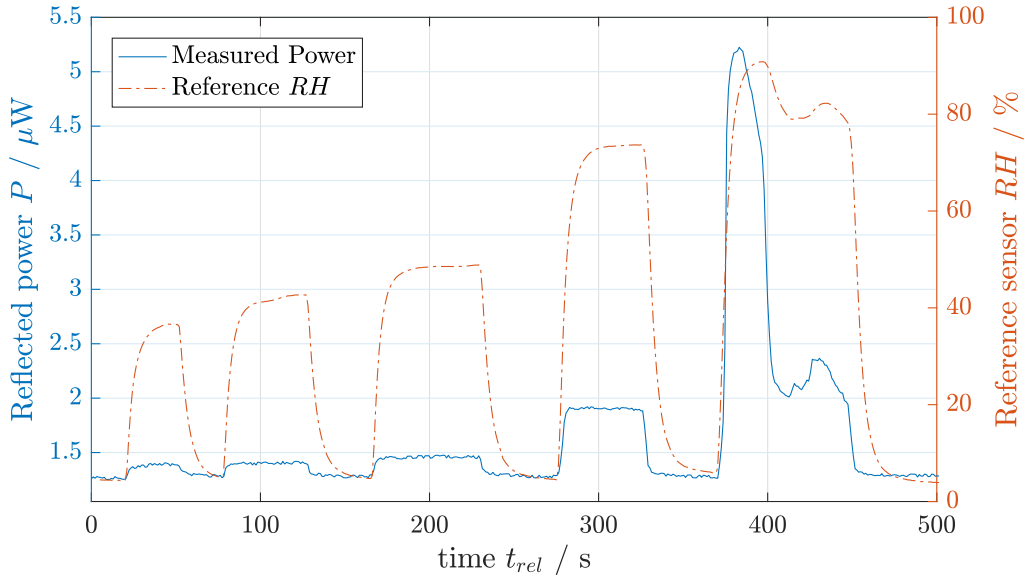

Figure 13: Measured reflected laser power (left axis - blue solid line) and RH, measured with the reference humidity sensor (right axis - red dash-dot line), over time for the deposition sample no. 1 at an incident angle of 60.5° (Brewster angle)

The reference sensor does not just display the RH value, but also the temperature over time, which is shown in figure 14. Together with the temperature it would be possible to calculate also the absolute humidity, but it is not in the scope of this work.

Figure 14 shows, that the temperature does change when the humidity is increased, but just within a small range of 0.2 °C. Hence, the requirement for an sufficiently stable temperature of the humid air coming from the humidity generator is fulfilled with the actual setup. At room temperature the equilibrium vapor pressure changes about 2 hPa/°C [35]. Together with equation (2), this would lead to a moderate difference in the relative humidity of less than 0.8 %RH, which is acceptable for the actual measurements. The temperature was about 24 °C for all measurements and showed similar behavior. Therefore, the temperature plot is shown just once.
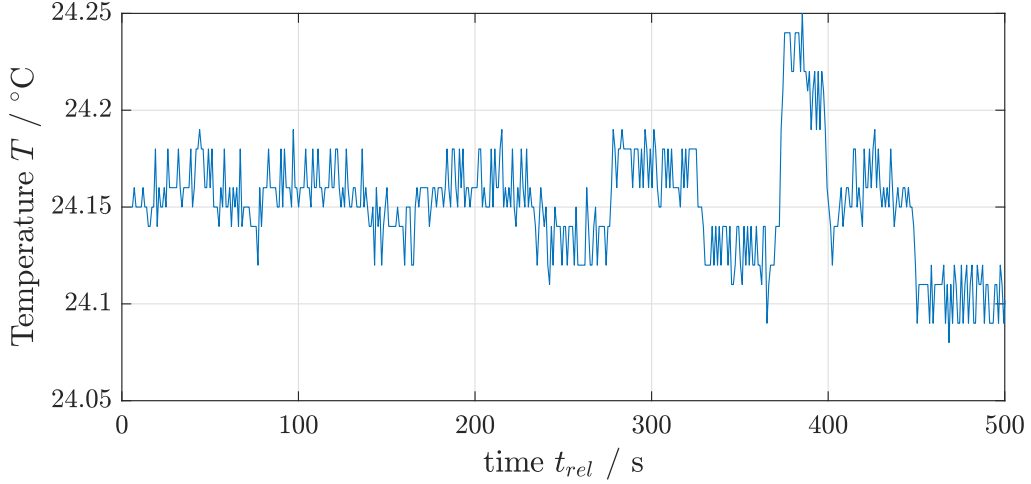

Figure 14: Temperature over time measured with the humidity reference sensor for the measurement shown in figure 13

A further measurement is performed at an incident angle of 45.05° to investigate the power signal tendency and is plotted in figure 15. The correlation between the reflected laser power and the reference RH value is again clearly visible, but contrary compared to the measurement at 60.5°. An increase of RH causes a decrease of the reflected laser power signal. Obviously, the interference pattern got shifted like predicted in section 3.3. It is already expected, that the signal behaves not like plotted in figure 6 for an incident angle of 45.05°. To get exactly the theoretically derived pattern, that angle ought to be adjusted with a clearance of ±0.001°, which is impossible even with the precision rotary stage. The effect of a small change of the incident angle over about 0.2° can be seen at $t_{rel} \approx 390$ s. The reflected power changes several times from a maximum to a minimum with $\Delta P \approx 15$ µW, which is about 30 % of the mean reflected power.

The curve after $t_{rel} = 400$ s represents the reflected power at a fixed, but slightly different incident angle, compared to the state before the angular variation. Apparently, the signal for low RH starts at a higher position, but still drops if the humidity and thus the thickness increases.
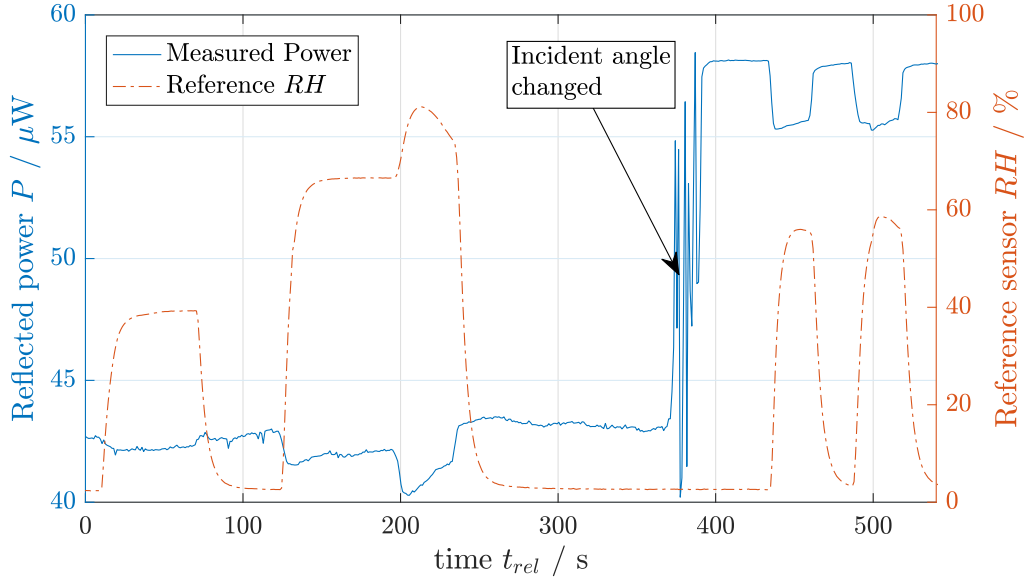
Figure 15: Measured reflected laser power (left axis - blue solid line) and RH, measured with the reference humidity sensor (right axis - red dash-dot line), over time for the deposition sample no. 1 at an incident angle of 45.05°. At 380 s the incident angle is changed over about $+0.2°$

A further measurement shows, that the high angular sensitivity also occurs at the Brewster angle (figure 16), which is in contrast to the theoretic model. This implies, that the reflection at the initial interface is not almost zero like expected. It can be caused either by the limited filter efficiency of the polarizers, as well as by the fact, that the Brewster angle is a theoretic model and a fully p-polarized light still gets slightly reflected. Therefore, polarizer sheets are added to the light path to maximize the grade of polarization. The effect of an angular change is again investigated. In figure 16 it can be seen, that not just the measured power drops after the insertion of polarizer sheet. Also the amplitude of the change in reflected power while shifting the angle decreases from about $\Delta P \approx 12\,\%$ of the mean reflected power at $t_{rel} \approx 300\,\mathrm{s}$ to $\Delta P \approx 6\,\%$ at $t_{rel} \approx 600\,\mathrm{s}$.
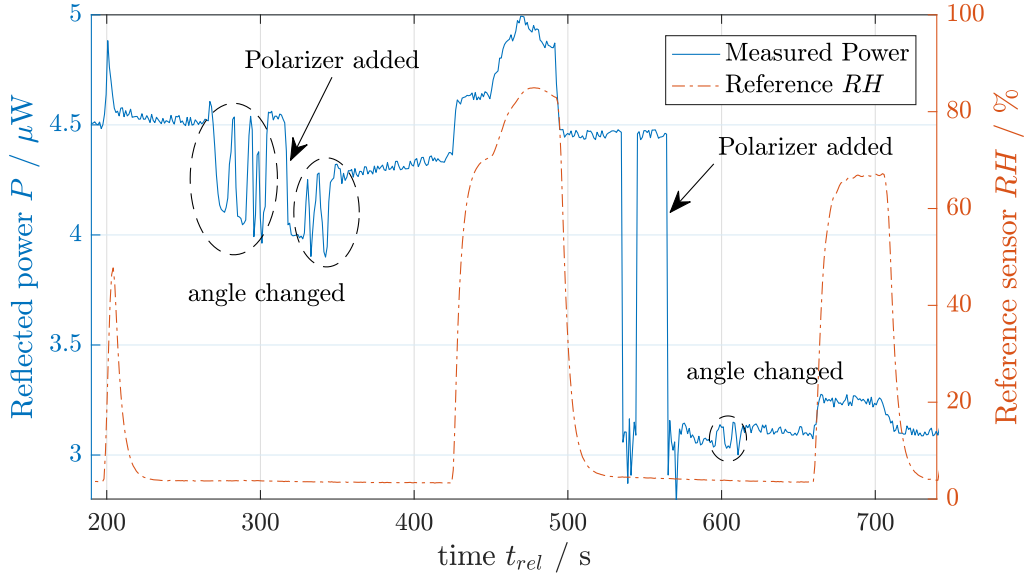
Figure 16: Measured reflected laser power (left axis - blue solid line) and RH measured with the reference humidity sensor (right axis - red dash-dot line) over time for the deposition sample no. 1 at an incident angle of 60.5°. At 380 s the incident angle is changed over about +0.2°. At certain times the incident angle is changed and polarizers are added.

Something which occurred in several measurements, that are not presented in this work, is an occasional shift of the reflected laser power over time, without variation of the RH value. This can be investigated from 350 s to 420 s in figure 16. Occasionally, this shift was almost 10 % of the mean signal, which is much more than the shift of the nominal laser power of 1 %, according to the specification sheet. It could be also determined by a minimal change of the incident angle due to vibrations or thickness changes of the thin film, that are not caused by humidity. The latter would be a serious problem for the whole measurement principle. It is not possible to discriminate between these effects with the applied laser interference setup. Hence, it was tried to perform measurements with the extended setup described in section 4.3.2 with deposition sample no. 1 to derive absolute thicknesses, which did not lead to satisfying results. Apparently the interfaces are not exact enough to generate an interference pattern that is sufficient to fit a thickness out of it. Also the ellipsometer measurements showed a rather high uncertainty. Therefore a new deposition with a similar configuration was performed, where the substrate was fixed to the bottom of the reactor by double sided tape. This strategy apparently increased the quality of the interfaces and lead to the results described in the following section.

5.2 Deposition Sample No. 2

The measurements shown in this subsection are performed with a sapphire window, coated on the 30.08.2017, and the extended setup, described in section 4.3.2, with the incident angle of the white light interference setup set to 36.8°. The thickness and optical properties of the thin film layer are measured with the ellipsometer and listed in table 4.

Table 4: Composition, thickness and optical parameters for the refractive index
(equation (32)) of the deposition sample no. 2 performed on the 30.08.2017

Property	Value
Amount of HEMA	100 %
Amount of EGDMA	0 %
Layer thickness	$(690.3 \pm 0.3)\,\mathrm{nm}$
Parameter A	1.514 ± 0.004
Parameter B	$(4.92 \pm 0.06) \times 10^{-3}$
Parameter C	0

In addition to the reflected laser power measured with the power meter, spectra of
the reflected white light are captured at crucial points. The theoretic reflectance
spectrum in figure 7 shows the ratio between reflected and incident intensity. Also
the measurements are performed the same way, because the intensity of the light
source, the transmission coefficients of the fiber and the sensitivity of the spectrom-
eter are not uniform over the wavelength range. The raw spectrum of the used
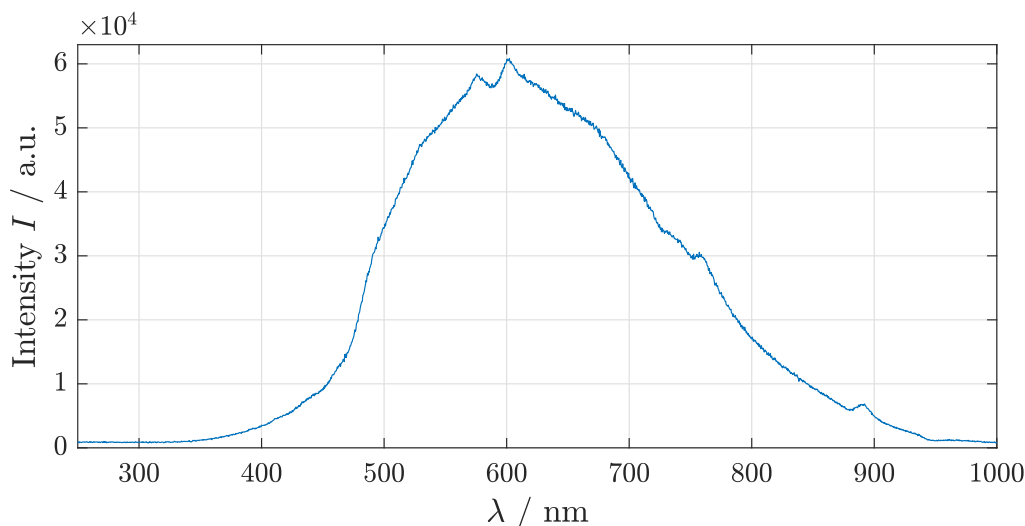measurement setup is plotted in figure 17.

Figure 17: Recorded raw spectrum of the tungsten halogen light source coupled with
fibers to the spectrometer

The applied spectrometer software (Ocean Optics OceanView) provides a special
reflectivity mode, that considers this incident intensity already during the capturing
process, according to equation (33).

$$R = \frac{I_r - B}{I_i - B} \tag{33}$$

R ... reflectance; I_r ... reflected intensity; I_i ... initial intensity; B ... background
intensity

The initial intensity is acquired before the real measurement. In the actual case, the
reflected light is much lower in intensity than the incident one. Therefore, not ex-

actly the incident intensity is recorded, but the reflected intensity from an uncoated sapphire window, in order to minimize the dynamic range of the measurement. The background intensity is measured, while the tungsten halogen lamp is blanked with a shutter and should compensate any stray light from the surroundings. When both measurements are completed, the software computes the reflectance from the measured reflected intensity in real time and displays the spectrum like shown in figure 18. It shows the spectrum over a wavelength range from 250 nm to 1000 nm.

For the determination of the thin film thickness, a least-squares fit with the model (equation (34)) is implemented in *Matlab* within a range of 400 nm to 800 nm. This is the regime, where the interference pattern is clearly observable. The function used for the fit is based on the theoretic model (equation (31)) and stated in equation (34) with the fit parameters C_1, C_2 and d_f. The wavelength dependent refractive index n_f for the thin film is calculated with the measured parameters from table 4, used in equation (32) and n_s for the substrate is taken from [36]. The incident angle of the white light $\theta_{0,w}$ is set to 36.8°. The uncertainty of the film thickness is dependent on the mean squared error (MSE) of the fit and determined by the Jacobian (95 % confidence interval).

$$R_{fit}(C_1, C_2, d_f) = C_1 + C_2 \cos\left(\frac{4\pi}{\lambda} d_f \sqrt{n_f^2(\lambda) - n_s^2(\lambda) \sin^2 \theta_{0,w}}\right) \tag{34}$$

$R_{fit}(C_1, C_2, d_f)$ ... fit function for the reflectance; C_1, C_2 ... linear offset parameter; d_f ... film thickness; λ ... wavelength, $\theta_{0,w}$ ... incident angle of the white light
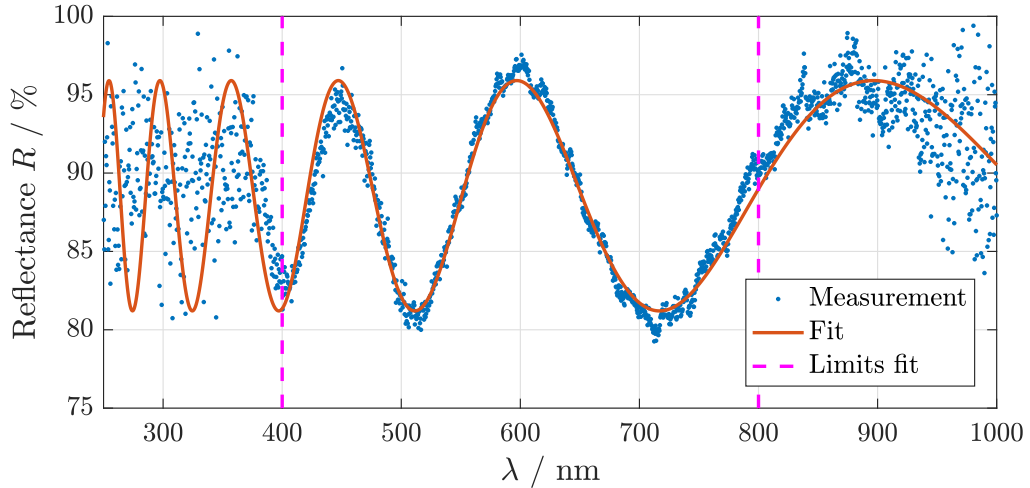

Figure 18: Spectrum of the reflected white light for deposition sample no. 2. For the determination of the thin film thickness, a least-squares fit with equation (34) is performed for the points within 400 nm to 800 nm. $d_f = (644.8 \pm 0.4)$ nm; MSE = 0.97. The result for linear offset parameters C_1, C_2 is not important

The model assumes, that the refractive index stays constant over the applied humidity range. This seems to be a valid assumption for humidity levels below 90 %RH, where the the fit matches the measured values well. Thus, the MSE and the uncertainty of the thickness are rather low like in figure 18. However, the quality of the fit obviously decreases for very high *RH* values. This can be investigated in

figure 19 for a spectrum recorded at 96 %RH. The MSE of the fit is rather high and therefore also the uncertainty of the fitted thickness gets worse. If the refractive index of the hydrogel is changed manually, the alignment could be improved. Apparently, the refractive index of the thin film varies with the increasing amount of water in the hydrogel. It would be possible to extent the parameter space of the fit with the refractive index. The problem of this approach is the ambiguity of the optical path length, which is the distance times the refractive index. A variation of the thickness can be compensated with the refractive index, which is a problem for an automated fitting routine. This ambiguity can be overcome by recording of spectra at several incident angles, like it is done in many ellipsometers. However, this cannot be performed with the applied measurement setup. Bigger uncertainties are considered for the worse quality of the fit. Furthermore, the MSE is used as an indicator, if the data is still useful. Just fits with a MSE < 20 are considered for the later evaluation.
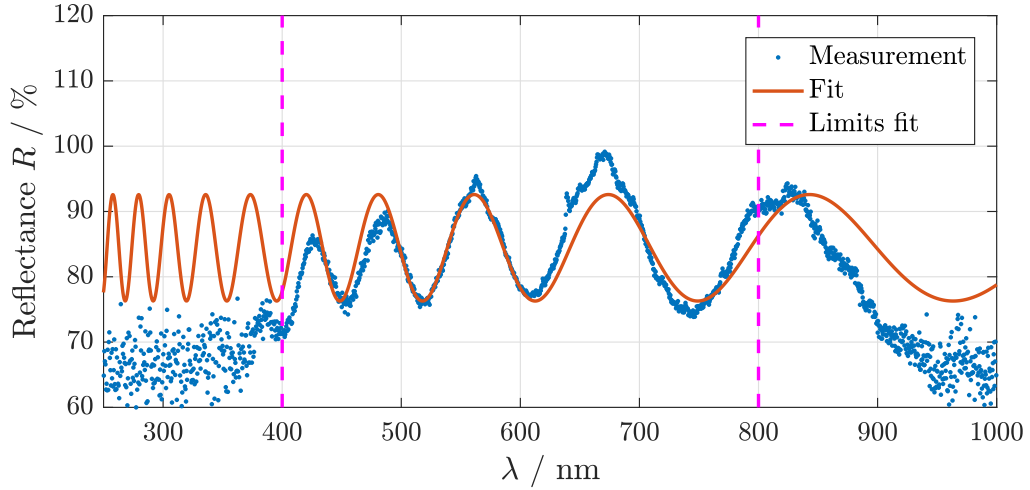

Figure 19: Spectrum of the reflected white light for deposition sample no. 2. The same fit as in figure 18 is applied at a humidity level of about 96 %RH to demonstrate the decreasing quality of the fit. Resulting $d_f = (1212 \pm 8)$ nm; MSE $= 14$

In contrast to the laser power measurement and the reference humidity sensor, that provide a sampling rate of 1 s, the recordings of the spectra are triggered manually at certain times and evaluated with the self-developed *Matlab* script.

Figure 20 shows the result of a measurement where all three values are captured simultaneously. A correlation of the signals is clearly visible. For a better comparability, the axis of the reflected laser power is inverted. The reflected laser power (blue curve) decreases with increasing reference RH (red curve). This aligns better with the predictions than deposition sample no. 1. The correlation is again not linear, but contrary to deposition sample no. 1, the power decrease flattens at higher RH. A non-linearity can be also seen between the reference RH (red) and the fitted absolute film thickness (green), although the increase of the thickness is higher than the one of RH. This implies, that the reflected laser power reaches a minimum of the theoretic interference pattern (figure 5) at the applied humidity of about 50 %RH. A further investigation is done in section 6.1.
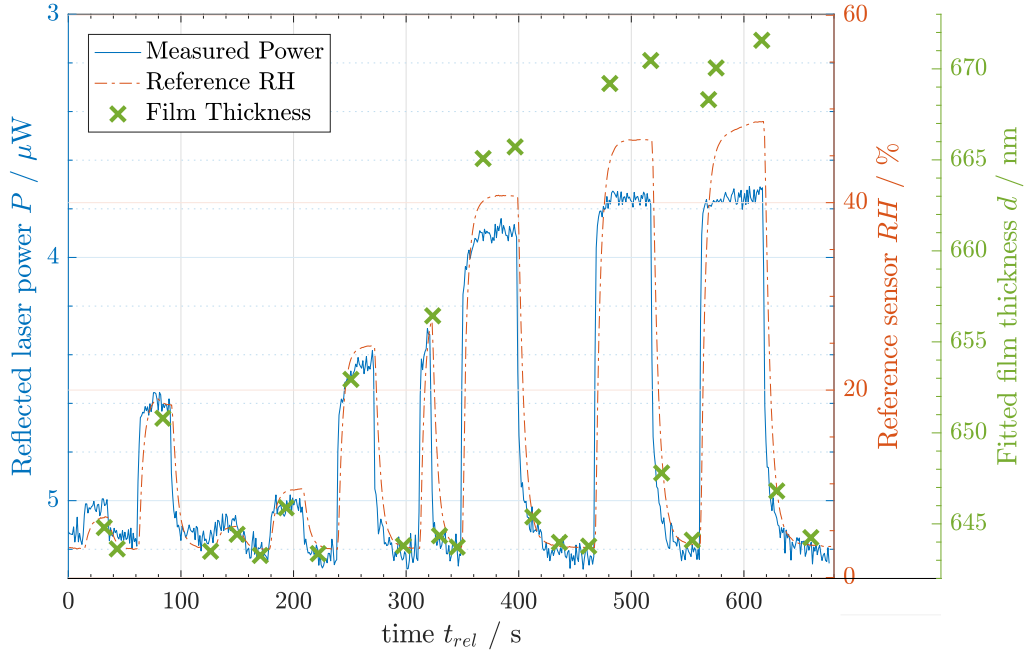
Figure 20: Measured reflected laser power (blue solid line), RH measured with the reference humidity sensor (red dash-dot line) and the film thickness fitted from recorded spectra (green points) over time for the deposition sample no. 2 at an incident angle of 60.5° of the laser. Note: The reflected laser power axis (blue) is inverted

Whereas figure 20 is focused on the humidity range lower than 50 %RH, figure 21 shows mainly the behavior of the setup for humidities above 50 %RH. Except of a small bump at around 400 s, the humidity is constantly increased up to a maximum of 97 %RH, according to the reference sensor (red curve). The fitted film thickness (green curve) has the same trend. Especially after 80 %RH, the thickness increase rises dramatically compared to lower RH values. It changes from 800 nm to 1400 nm within the range from 80 %RH to 97 %RH. Below 80 %RH, the thickness increase is just from 650 nm to 800 nm. This confirms the non-linearity further. Also the reflected laser power signal (blue curve) shows a immense variation while the increase of RH. Obviously, the power signal follows an interference pattern like expected. A further investigation, if it aligns with the theoretic model, is done in section 6.1. Something remarkable occurs after 600 s. The laser signal abruptly drops and stays almost constant. The recorded spectra of the white light reflectance cannot be fitted anymore, because the interference pattern disappeared almost entirely. Apparently, the hydrogel thin film started to dissolve at the applied high RH values. For an actual sensor implementation, this would provoke a problem, because it is a non-reversible process and damages the thin film completely. Nevertheless, for the evaluation of the hydrogel, this is a useful information and is discussed in more detail in section 6.3.
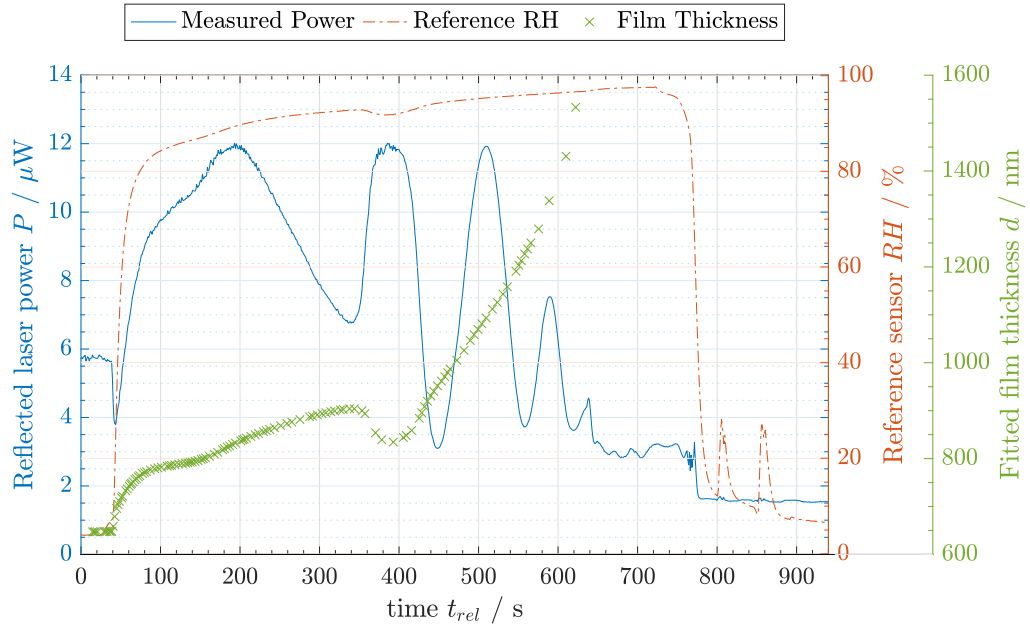
Figure 21: Measured reflected laser power (blue solid line), *RH* measured with the reference humidity sensor (red dash-dot line) and the film thickness fitted from a recorded spectrum (green points) over time for the deposition sample no. 2 at an incident angle of 60.5° of the laser.

6 Discussion

From the data captured in section 5, correlations between the measured quantities can be clearly observed. Nevertheless, some uncertainties concerning the behavior of the reflected power signal need a deeper investigation, like the signal increase instead of a decrease. Apparently, the reflection at the initial interface is not almost zero at the Brewster angle and causes a shift of the interference pattern. In this chapter the correlations are investigated in more detail.

6.1 Verification of Laser Interference Model

In section 5 it is already assumed, that there are slight deviations in the measurements from the ideal interference model. In this section, the behavior of the reflected laser power signal is investigated in more detail.

6.1.1 Deposition Sample No. 1

The measurements in figure 13 show, that the theoretic interference pattern (figure 5) apparently does not perfectly apply for the measured values. However, by measuring just the reflected laser power it is hard to determine, if the change in the signal is caused just by variation of the thickness or by other influences. Measurements with the extended setup could not be performed with deposition sample no. 1, so a deeper investigation of the signal behavior was not possible.

6.1.2 Deposition Sample No. 2

With the extension of the setup introduced in section 4.3.2, it is possible to analyze the model, because the absolute thickness and the reflected laser power is measured simultaneously. The relation between these two quantities is exactly what the laser interference model describes. Deposition sample no. 2 allowed to perform these measurements as plotted in figure 21. Figure 22 shows the result of the measured values taken from figure 21 in comparison to the ideal, theoretic model. At first sight, the deviation of the measured values from the ideal model looks quite immense. To investigate how the measured values still can be explained by the model, a fit is applied, which is described by equation (35). In section 5.1 it is already suspected, that the reflection at the initial interface is apparently not close to zero, like expected in the model. Therefore, the electric field, that is reflected from that interface, is multiplied by a correction factor. Considering that factor, already slight changes of the incident angle cause a shift of the interference pattern. Hence, the angle of incidence is also a fit parameter. The offset parameter is needed to consider stray light, that causes a uniform shift of the reflected power.

$$P_{r,fit}(D_1, D_2, \theta_0) = D_1 + |D_2 \, E_{0r}(\theta_0) + E_{1r}(\theta_0) + E_{2r}(\theta_0)|^2 \qquad (35)$$

$P_{r,fit}(D_1, D_2, \theta_0)$ ... fit function for the reflected laser power; D_1 ... offset parameter; D_2 ... correction factor for the reflection at the initial interface; θ_0 ... incident angle; $E_{0r}(\theta_0), E_{1r}(\theta_0), E_{2r}(\theta_0)$ ... angular dependent reflected electric fields
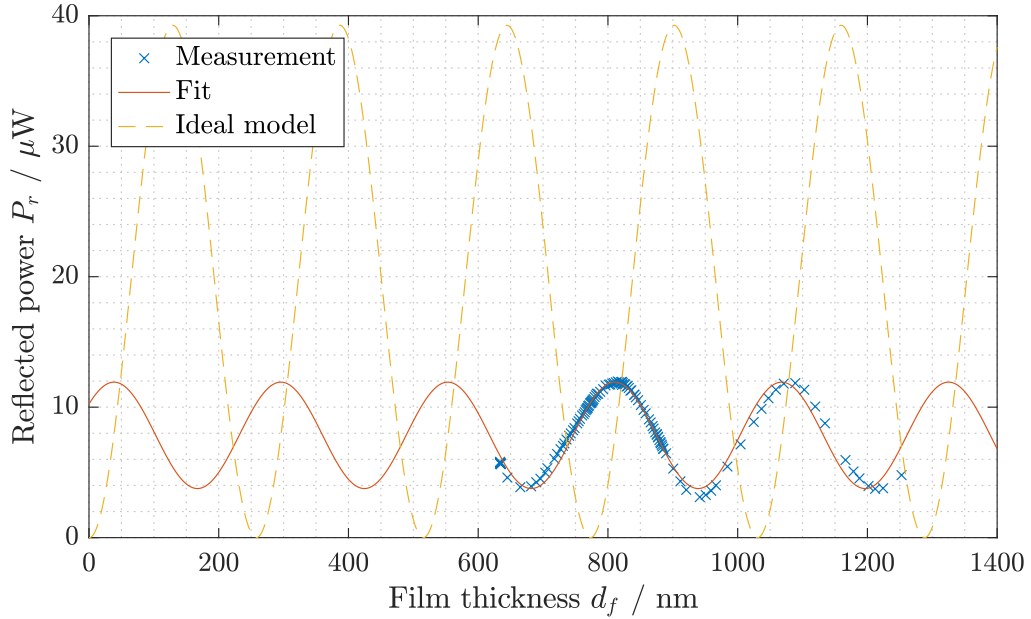
Figure 22: Measured reflected laser power as a function of the absolute thickness at the Brewster angle as incident angle (blue crosses) in comparison with the ideal interference pattern, calculated with equation (19) (yellow dashed curve) for an incident laser power of 4.6 mW. The solid red curve shows the least-squares fit for the modified model described with equation (35). Result for the fit parameters:
$$D_1 = -1.37,\ D_2 = 25.10 \text{ and } \theta_0 = 60.31°$$

Considering all three parameters, the fit describes the measured values shown in figure 22 nicely. The small deviations could be explained by a slightly different refractive index of the hydrogel caused by wetting, that is not taken into account by the model. The parameters computed with the fit show just one possible solution. Since a change of the initial angle of just $0.02°$ changes the phase of the interference pattern over one period, there are more solutions possible within the applied boundaries from $60.3°$ to $60.5°$. The fit just displays the fact, that it is possible to describe the measurement with some reasonable modifications of the theoretic model. The actual values of the parameters are not that important.

Additionally, figure 22 shows, that the assumed thickness increase of 30 % is far too small for the applied hydrogel and visualizes another problem. The proposed measurement principle just works out with monotonic functions, because otherwise the mapping from a measured power to a thickness is ambiguous. So, for a periodic function, like in the actual case, the measurement range has to be restricted to half a period. Otherwise, different thickness values are possible for a measured power value. The total thickness increase is apparently about 100 %. This leads to an increase over two periods for an initial thickness of approximately 630 nm and a 635 nm laser. Thus, for an actual sensor application the current configuration is not applicable. Former measurements of Unger et al. [13] show, that the increase can be limited by a higher amount of EGDMA in the polymer composition, which also prevents the thin film from dissolving at high humidity levels. Hence, for an actual implementation such p(HEMA-co-EGDMA) hydrogels are expected to be more suitable.

6.2 Response Time

One of the demands, defined in the objective for the newly developed humidity measurement system, is a fast response to an abrupt increase of the surrounding humidity level. Both depositions show a fast response to an abrupt change of the surrounding humidity level.

6.2.1 Deposition Sample No. 1

In figure 13, a faster response than the reference humidity sensor can be already observed. Especially the signal drops reveal much faster response rates than the reference sensor. Also the signal increase of the hydrogel sensor is faster than the reference, but harder to observe in this plot. A more detailed investigation is done in the following subsection.

6.2.2 Deposition Sample No. 2

For a deeper analysis, the signals from figure 20 at $515\,$s are plotted in more detail in figure 23, with $t_{ref} = 0$ shifted to the start of the signal drop. The manufacturer of the reference sensor defines the response time as the time, at which the sensor readings change $63\,\%$ of the full RH step [37]. This is an exponential decrease with the time constant τ_{63}. This constant is declared as $\tau_{63} < 8\,$s for the applied reference sensor [10].

Figure 23 shows, that the response time for a signal drop from $47\,\%$RH to $3.5\,\%$RH of the reference sensor is about $\tau_{63,ref} = (7.8 \pm 0.5)\,$s, which is in good agreement with the specification. The reflected power signal reaches the corresponding bottom value in about $\tau_{63,pow} = (2.5 \pm 0.5)\,$s. This is almost three times faster than the reference. The shape of the drop of the humidity setting is just a theoretic estimation and might deviate about $1\,$s, when the pumping speed and the air volume of the whole system are considered.

The same analysis can also be performed for the sudden increase from $3.5\,\%$RH to $47\,\%$RH of the humidity setting at $470\,$s from figure 20 and is shown in figure 24. The response of the reference sensor is $\tau_{63,ref} = (6.2 \pm 0.5)\,$s and of the reflected laser power signal $\tau_{63,pow} = (1.5 \pm 0.5)\,$s. Again, the optical setup is much faster than the reference. In comparison with the humidity decrease, the response time for the increase is about 20 to $40\,\%$ faster. The same effect is observed for thermo-responsive polymers, where the deswelling happened with a longer time scale than the swelling process [38].
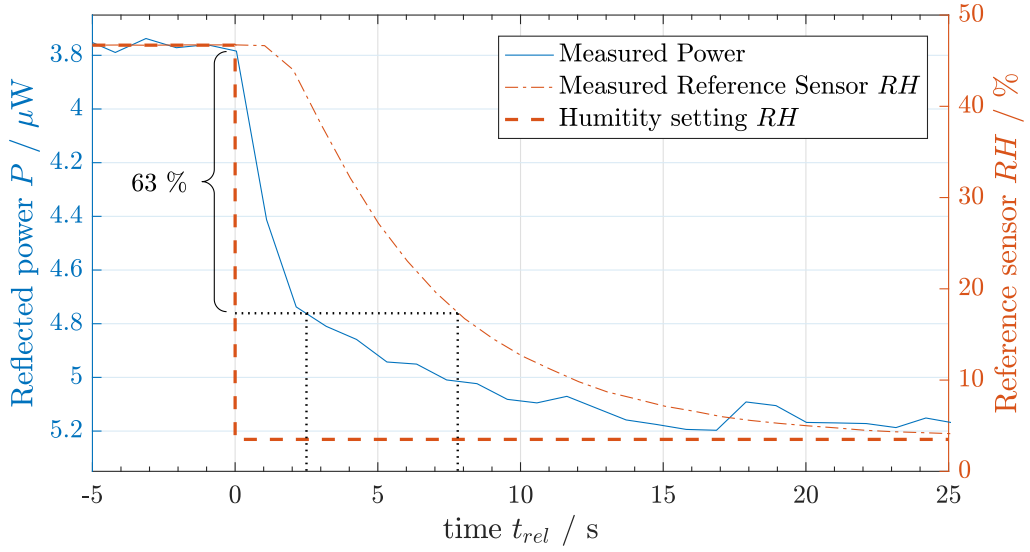
Figure 23: Measurement of the response time of the reflected laser power (blue solid curve) $\tau_{63,pow} = (2.5 \pm 0.5)\,\text{s}$ and the RH signal measured with the reference sensor (red dash-dot curve) $\tau_{63,ref} = (7.8 \pm 0.5)\,\text{s}$ after a drop of the humidity setting from $47\,\%\text{RH}$ to $3.5\,\%\text{RH}$
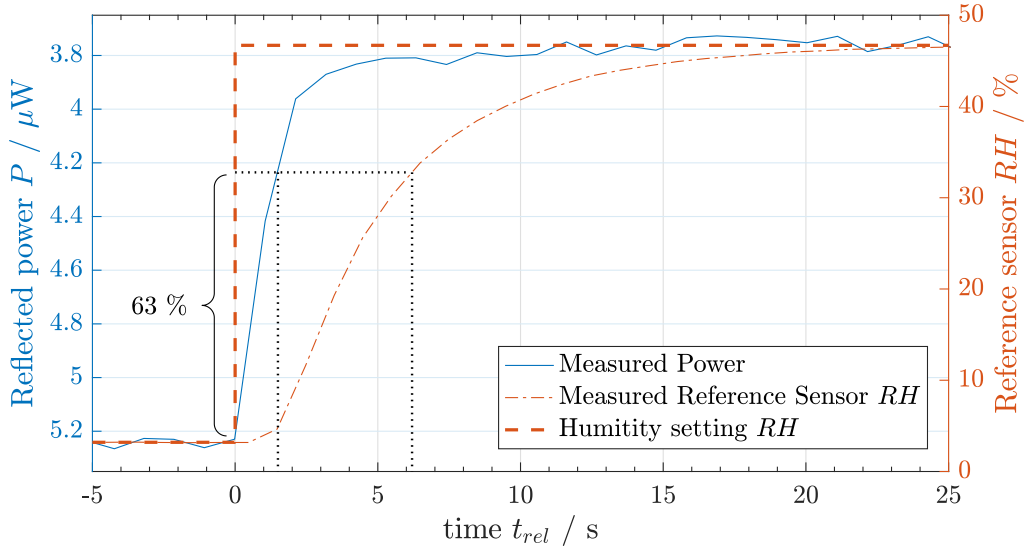

Figure 24: Measurement of the response time of the reflected laser power (blue solid curve) $\tau_{63,pow} = (1.5 \pm 0.5)\,\text{s}$ and the RH signal measured with the reference sensor (red dash-dot curve) $\tau_{63,ref} = (6.2 \pm 0.5)\,\text{s}$ after a rise of the humidity setting from $3.5\,\%\text{RH}$ to $47\,\%\text{RH}$

Concluding this section, the response times of the hydrogel sensor are much faster than expected from previous measurements. It is assumed, that the limiting factor is the thin film thickness, meaning that thinner films would lead to response times even below one second. Such fast sensors would enable an application for high dynamic processes like breath monitoring in medical research.
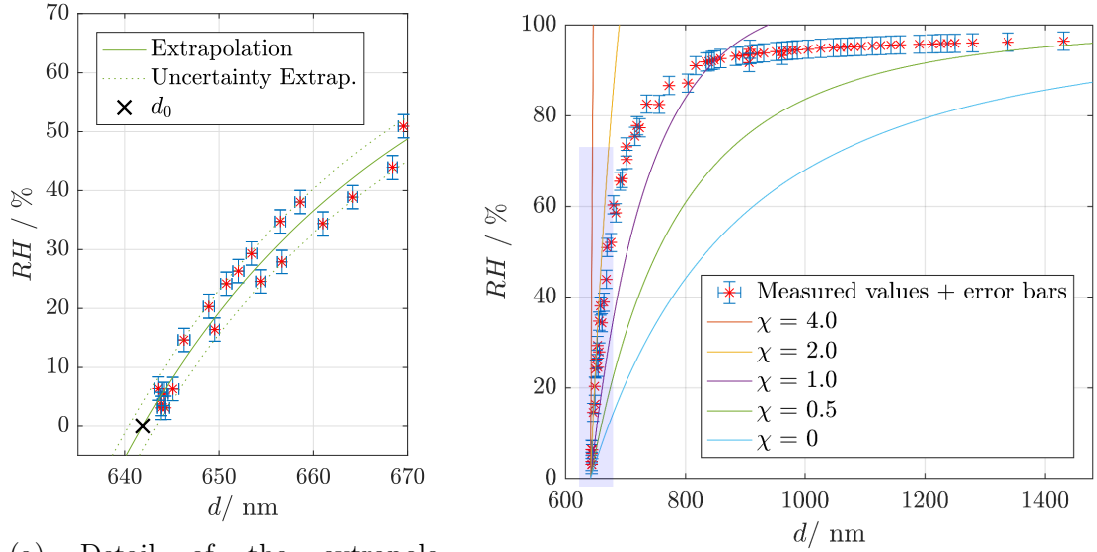
41

6.3 Application of Flory Huggins Theory

It is necessary to apply the Flory Huggins theory, like explained in section 3.1.1, for a relation of a measured thin film thickness of the hydrogel to a RH value. This is the most crucial relation for a later sensor application, because it translates the measured value (thickness) to the value that is supposed to be observed (RH). For an application of that theory, the Flory Huggins parameter χ must be empirically determined, which is done in this section.

6.3.1 Deposition Sample No. 1

A deeper investigation of the Flory Huggins Theory is not possible with the laser interference setup, because unique mapping from the power signal to a thickness value cannot be performed, which is explained in section 6.1. The discussion in this section is based on the absolute thickness values, that are determined by the simultaneously recorded spectra of the reflected white light. As explained in section 5.1, a measurement of absolute thicknesses with the extended setup could not be performed with deposition sample no. 1.

6.3.2 Deposition Sample No. 2

Measuring absolute thicknesses with the extended setup was possible without any problems with deposition sample no. 2. In figure 25b certain RH values are plotted as a function of the thin film thickness d, taken from calibration measurements, where the humidity is slowly varied to ensure, that the reference sensor also reaches its plateau value. These measurements are also used for the evaluation (figure 29, 30 and 32). In order to investigate the Flory Huggins theory (equation (9)), it is necessary to determine the initial thickness d_0 at $0\,\%$RH. Since the lowest RH value that could be reached is about $3\,\%$RH, this thickness is not detected experimentally, but derived by extrapolation of the data shown in figure 25a with *Matlab*. This is performed by regression of an extrapolation function, that is based on equation (9) with χ polynomial expanded in terms of the thickness. The resulting thickness is $d_0 = (641.9 \pm 1.4)\,$nm. The uncertainty is determined by the Jacobian of the regression. With that initial thickness d_0, it is possible to investigate equation (9) in more detail. Unfortunately, it is not possible to bring it in a closed from, because the Flory Huggins parameter χ is dependent on RH and d_0/d respectively. Theoretic curves for different values of χ are plotted in figure 25b. It can be seen, that χ decreases with increasing RH.

(a) Detail of the extrapolation function and the intersection with $0\,\%\mathrm{RH}$ that marks $d_0 = (641.9 \pm 1.4)\,\mathrm{nm}$

(b) Overview over the whole measured data. The solid curves are solutions of equation (9) for different χ values

Figure 25: Relative humidity (RH) measured with the reference sensor as a function of the absolute thickness measured with the spectrometer. The uncertainty of RH is defined by the specification of the sensor and of the thickness by the quality of the fit, like described in figure 18. Figure (a) is the detail of the blue shaded area of (b)

Equation (9) can be rearranged to derive an expression for χ as a function of the measured values, which is shown in equation (36) and the corresponding plot in figure 26a. The error bars are determined by standard error propagation (equation (37)) with the uncertainties of the measured values. According to the specifications, it is $\pm 2\,\%\mathrm{RH}$ [34] for the reference humidity sensor. The uncertainty of the thickness is determined by the Jacobian of the fit of the reflectance spectrum (95 % confidence intervals). Due to the small changes in thickness at low humidity levels, the uncertainties for χ are quite large in that range. Anyway, the result depicted in figure 26 is in good alignment with the work of Unger et al. [13], where just the range between 70 to $85\,\%\mathrm{RH}$ is measured (figure 26b). Their predictions for humidity levels smaller than $70\,\%\mathrm{RH}$ are apparently not valid for the results of the recent experiment, shown in figure 26a.

$$\chi_{meas} = \frac{\ln\left(RH\right) - \ln\left(1 - \frac{d_0}{d}\right) - \frac{d_0}{d}}{\left(\frac{d_0}{d}\right)^2} \tag{36}$$

χ_{meas} ... Flory Huggins parameter; RH ... measured relative humidity; d_0 ... measured initial thickness of the polymer; d ... measured actual thickness of the polymer;

The corresponding uncertainty calculation, according to the standard error propagation applied on equation (36), is carried out in equation (37):
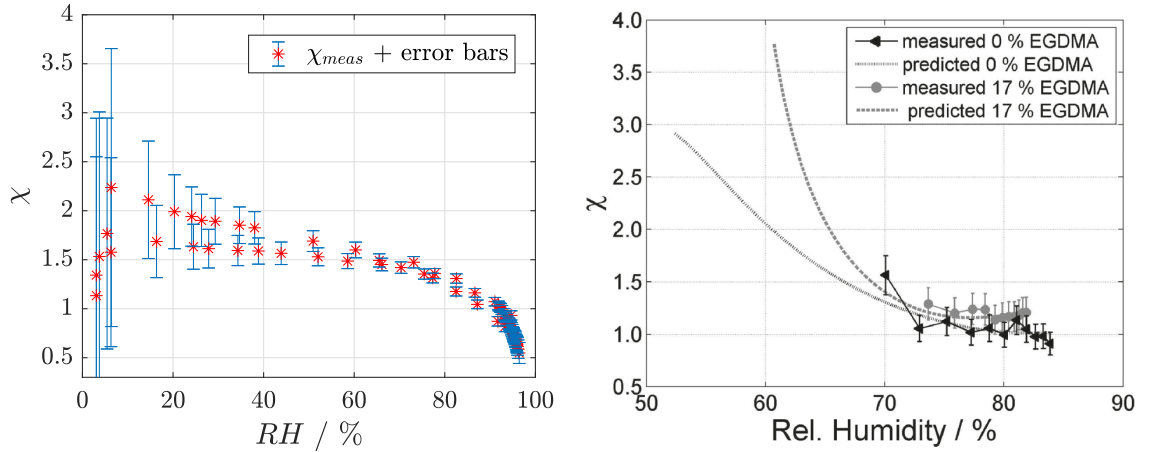
$$\Delta \chi_{meas} = \left| \frac{\partial \chi_{meas}}{\partial RH} \right| \Delta RH_{meas} + \left| \frac{\partial \chi_{meas}}{\partial \left(\frac{d_0}{d} \right)} \right| \Delta \left(\frac{d_0}{d} \right)$$

$$\Delta \chi_{meas} = \left| \frac{1}{RH \left(\frac{d_0}{d} \right)^2} \right| \Delta RH_{meas}$$

$$+ \left| \frac{\left(\frac{d_0}{d} - 2 \right) \frac{d_0}{d} / \left(\frac{d_0}{d} - 1 \right) + 2 \ln(1 - \frac{d_0}{d}) - 2 \ln(RH)}{\frac{d_0}{d}} \right| \Delta \left(\frac{d_0}{d} \right) \qquad (37)$$

with

$$\Delta \left(\frac{d_0}{d} \right) = \left| \frac{1}{d} \right| \Delta d_0 + \left| \frac{d_0}{d^2} \right| \Delta d \qquad (38)$$

$\Delta RH_{meas} = 0.02$ ... uncertainty of the reference sensor [34]; $\Delta d_0 = 1.4\,\mathrm{nm}$ ... uncertainty determined by extrapolation (cf. figure 25a); Δd ... individual uncertainty of the measured thickness, derived by the fit like shown in figure 18 (95 % confidence interval)

(a) χ_{meas} computed with equation (36) using actual measured data

(b) Former measurement performed by Unger et al. [13]

Figure 26: Comparison of the Flory Huggins parameter χ dependent on the relative humidity RH with former measurements

Figure 26a shows another interesting feature. The data for RH values $> 95\,\%\mathrm{RH}$ is taken from the measurement plotted in figure 21, where dissolution of the thin film occurs for humidities $> 97\,\%\mathrm{RH}$. The minimum value for χ, that could be still computed with the measured data, is 0.55 ± 0.11. A reasonable measurement cannot be performed beyond that point, because the dissolution is already too far advanced. Theoretic models show, that for good solvents the value for χ must be less than 0.5, which denotes an approximate limit for dissolution. If the value is slightly larger than 0.5, it is expected, that the polymer is swollen by the solvent [39]. So, the observed swelling and final dissolution phenomenon with the drop of χ

to 0.5, is in good alignment with the literature.

Even if there is no analytic expression for the Flory Huggins parameter χ, an approximation must be found to relate the measured thickness values to a relative humidity RH. A common approach is a fit with a polynomial expansion of χ in terms of the volume fraction of the polymer [40], which is equivalent to the ratio of the initial thickness over the actual thickness of the hydrogel d_0/d. Equation (39) shows the expansion performed up to second order. The Flory Huggins parameter χ_{meas} is plotted as a function of d_0/d in figure 27. The error bars are determined by equation (37) and are rather high in the vicinity of $d_0/d = 1$. The amount of water is almost zero in that domain and thus the thickness increase is just a few nanometer. The uncertainty of the initial thickness d_0 is 1.4 nm. This leads to a very uncertain result for χ_{meas} in that area. Therefore, a weighted fit with equation (39) is performed in a *Matlab* script. The inverse of the individual uncertainty $\Delta\chi_{meas}$ is taken as weighting parameter. A second order polynomial fit looks quite reasonable with this strategy. The alignment of fit could be improved by including more terms in the polynomial, but applying higher orders is not common in the literature [41].

$$\chi = \chi_0 + \chi_1 \left(\frac{d_0}{d}\right) + \chi_2 \left(\frac{d_0}{d}\right)^2 \tag{39}$$

χ ... fit function for Flory Huggins parameter; χ_0, χ_1, χ_2 ... coefficients; d_0 ... initial thickness of the polymer; d ... actual thickness of the polymer;
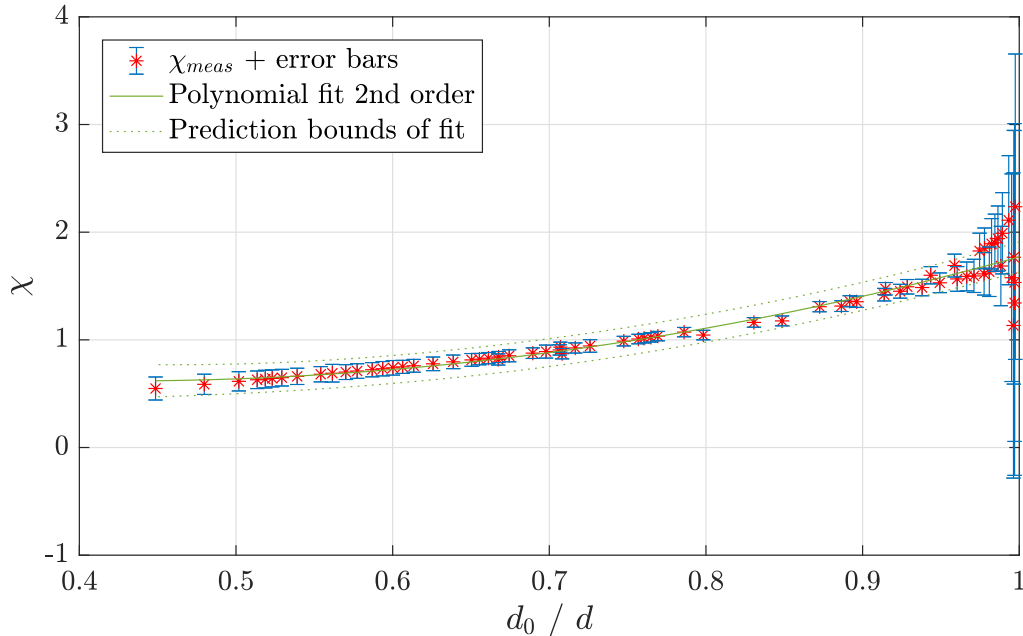

Figure 27: Flory Huggins parameter χ_{meas} computed with equation (36) over the thickness ratio d_0/d. A weighted polynomial fit of second order (equation (39)) is performed with the measured data points. The weights are defined as the inverse of the individual error $\Delta\chi_{meas}$. The 95 % prediction bounds for a new observation are a result of the Jacobian of the fit. Result for the fit parameters: $\chi_0 = 1.6 \pm 0.4$, $\chi_1 = -4.0 \pm 1.0$, $\chi_2 = 4.2 \pm 0.7$

The result of the least-squares fit for χ is shown in figure 27 with the corresponding polynomial coefficients $\chi_0 = 1.6 \pm 0.4$, $\chi_1 = -4.0 \pm 1.0$, $\chi_2 = 4.2 \pm 0.7$. The uncertainties are determined by the Jacobian of the fit. The dotted interval represents the 95 % prediction bounds for a new observation.

Inserting equation (39) in equation (9), with the parameters found by the fit shown in figure 27, leads to the final result for the relation of the thickness change to a RH value. The corresponding curve (solid green in figure 28) represents the conversion from the normalized thickness d/d_0 to RH. Figure 28 is a general relation and is valid for any pure HEMA thin film, because the abscissa is normalized by the initial thickness. This is an important result and denotes the basis for future sensor applications.

Figure 28 shows the measured values for RH over the normalized thickness d/d_0 in comparison with the calculated function for RH using the Flory Huggins parameter χ, derived by the fit. The error bars of the measured values are due to the uncertainty of the reference humidity sensor (± 2 %RH [34]) and the fit of the thicknesses. The uncertainty bounds for the calculated function are calculated with equation (40) by standard error propagation applied on equation (9) with an estimated uncertainty $\Delta d = \pm 1$ nm for the whole thickness range.

$$\Delta RH = \left| \frac{\partial RH}{\partial \left(\frac{d_0}{d} \right)} \right| \Delta \left(\frac{d_0}{d} \right) + \left| \frac{\partial RH}{\partial \chi} \right| \Delta \chi$$

$$\Delta RH = \left| \frac{d_0}{d} \exp \left(\frac{d_0}{d} + \chi \left(\frac{d_0}{d} \right)^2 \right) 2 \left(\frac{d_0}{d} - 1 \right) \chi + 1 \right| \Delta \left(\frac{d_0}{d} \right)$$

$$+ \left| - \left(\frac{d_0}{d} - 1 \right) \left(\frac{d_0}{d} \right)^2 \exp \left(\frac{d_0}{d} + \left(\frac{d_0}{d} \right)^2 \chi \right) \right| \Delta \chi \qquad (40)$$

$\Delta \chi$ ... uncertainty of the χ determined with the fit in figure 27; $\Delta \frac{d_0}{d}$ ... uncertainty of the thickness ratio determined by equation (38) for $\Delta d = \pm 1$ nm
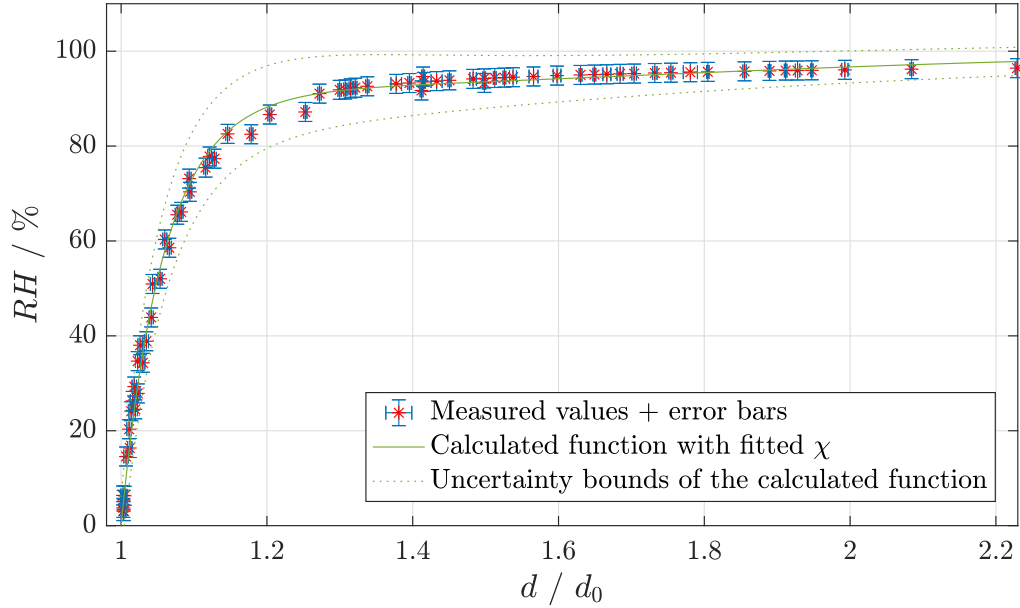
Figure 28: Calculated curve for RH (equation (39) inserted in equation (9)) as a function of the thickness ratio d/d_0 with the usage of the fitted function for χ, compared with the measured values for the reference RH and the simultaneously measured thicknesses. The uncertainty bounds are determined with equation (40) for estimated uncertainties of $\Delta d = \pm 1\,\mathrm{nm}$ for the whole range.

6.4 Evaluation Measurements

Since a direct conversion between the thickness and a humidity value RH is derived, an evaluation of this relation function can be performed.

6.4.1 Deposition Sample No. 1

The evaluation of the measurement just works out if the relative thickness of the thin film is known. A derivation of this relative thickness is not possible with the laser interference setup, which is explained in section 6.1. As explained in section 5.1, a measurement of absolute thicknesses with the extended setup could not be performed with deposition sample no. 1. Therefore, an evaluation of the measurements with respect to the reference sensor is not possible with this deposition.

6.4.2 Deposition Sample No. 2

Figures 29 to 32 show the result of a chronological series of humidity measurements with the thin film of deposition sample no. 2. At certain time points, the thickness and hence the corresponding RH value are calculated by the relation shown in figure 28 (with equation (39) inserted in equation (9)). The calculated RH values from the optical hydrogel sensor setup (red points) are compared with the RH values measured by the reference humidity sensor (solid green curve). The data used for the determination of χ (figure 27) is also taken from these measurements. The uncertainty of the computed RH values is calculated using equation (40) with the

uncertainty of χ shown in figure 27 and the individual uncertainty of d_0/d for every thickness measurement from the fit (like shown in figure 18). The error bounds of the reference sensor are $\pm 2\,\%$ according to the specifications [34].

Figure 30 shows the result for a stepwise increase of the relative humidity RH over a timescale of about 20 min. In general, the computed RH is in good alignment with the RH value, measured with the reference sensor, especially at higher RH values. There is a deviation of the mean values noticeable at low RH levels, but it is still within the error bars.
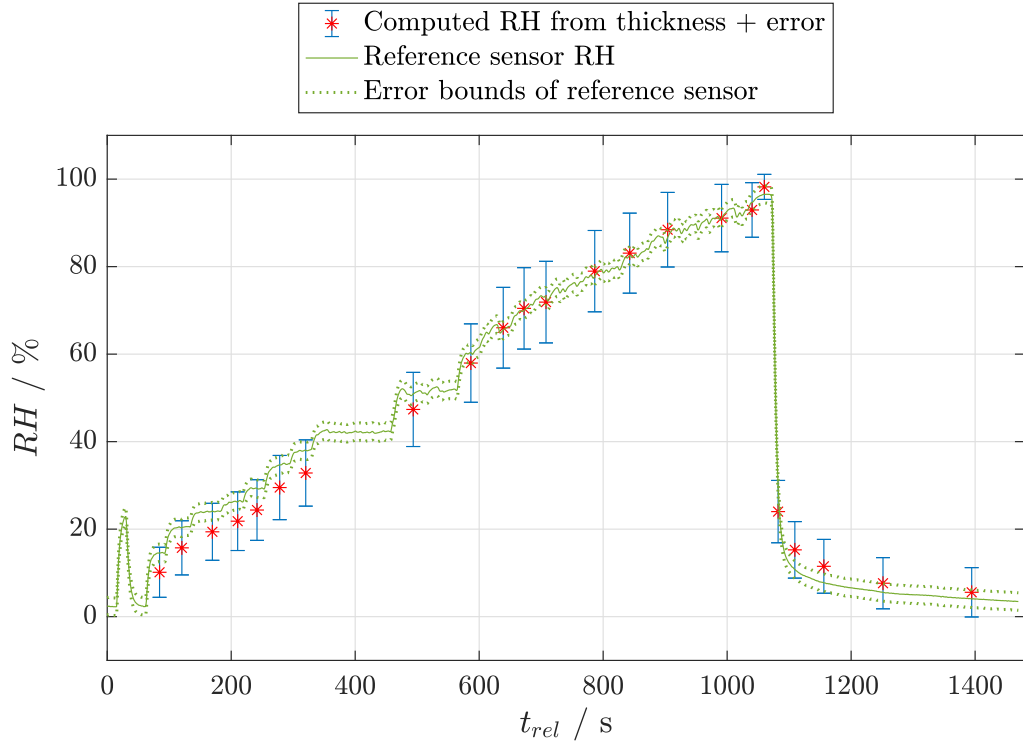

Figure 29: Evaluation measurement 1: Comparison of RH values, computed with the thickness of the hydrogel and RH, measured with the reference humidity sensor. Error bars are determined with equation (40) and the uncertainties for the actual thickness measurement. The uncertainty of the reference sensor is $\pm 2\,\%$ [34].

In figure 30, the computed RH values from the thickness measurement correlate again quite well with the reference sensor. The stepwise increase in this plot is faster compared to the previous one. Along the increase, the mean values of the computed RH tend to lie a bit higher than the reference. This could be caused by the inertia of the reference sensor, that is shown to be higher in section 6.2. Also for the first two measurements of the humidity decrease, it seems like the optical hydrogel sensor reacts faster than the reference. However, especially at the last two points the opposite is the case. Since the reference value is still within the error bars of the computed one, it is hard to determine, whether it is just measurement uncertainty or some kind of hysteresis behavior.
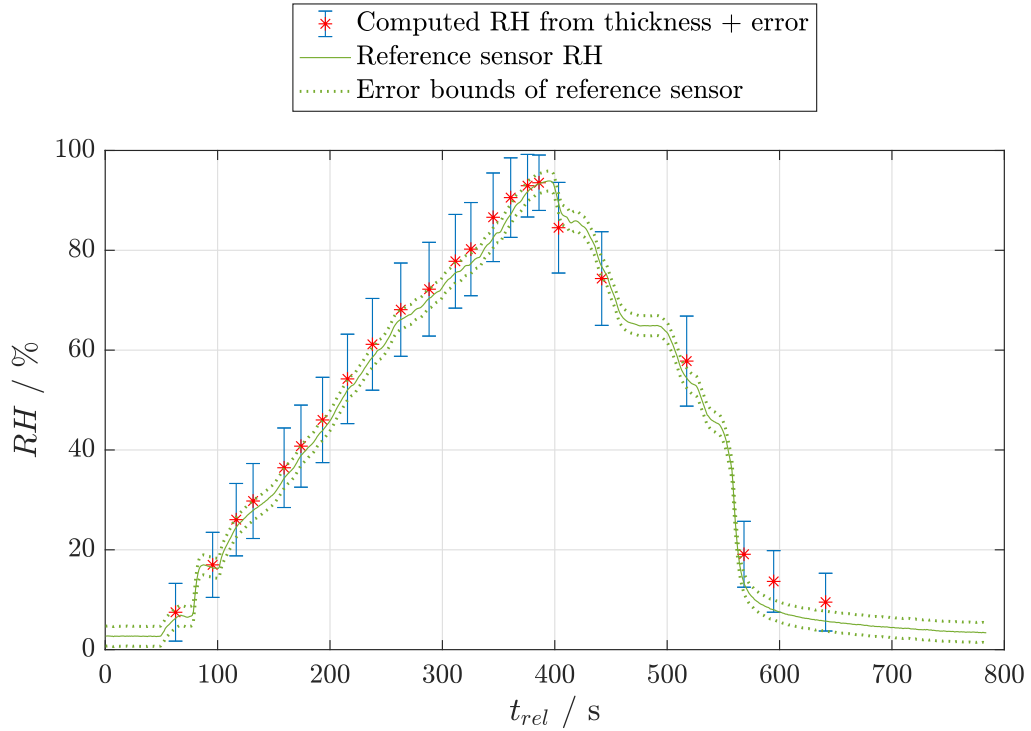

Figure 30: Evaluation measurement 2: Comparison of RH values, computed with the thickness of the hydrogel and RH, measured with the reference humidity sensor. Error bars are determined with equation (40) and the uncertainties for the actual thickness measurement. The uncertainty of the reference sensor is $\pm 2\,\%$ [34].

The measurement in figure 31 is already presented in section 5.2 as a raw data plot. Both datasets (computed RH and reference RH) are in good alignment within the error bar. Also with this approach the response of the hydrogel setup seems to be faster than the reference, but is hard to investigate, due to the low density of recordings for the computed RH. A hysteresis can be neither verified nor precluded with the results after the several signal drops.
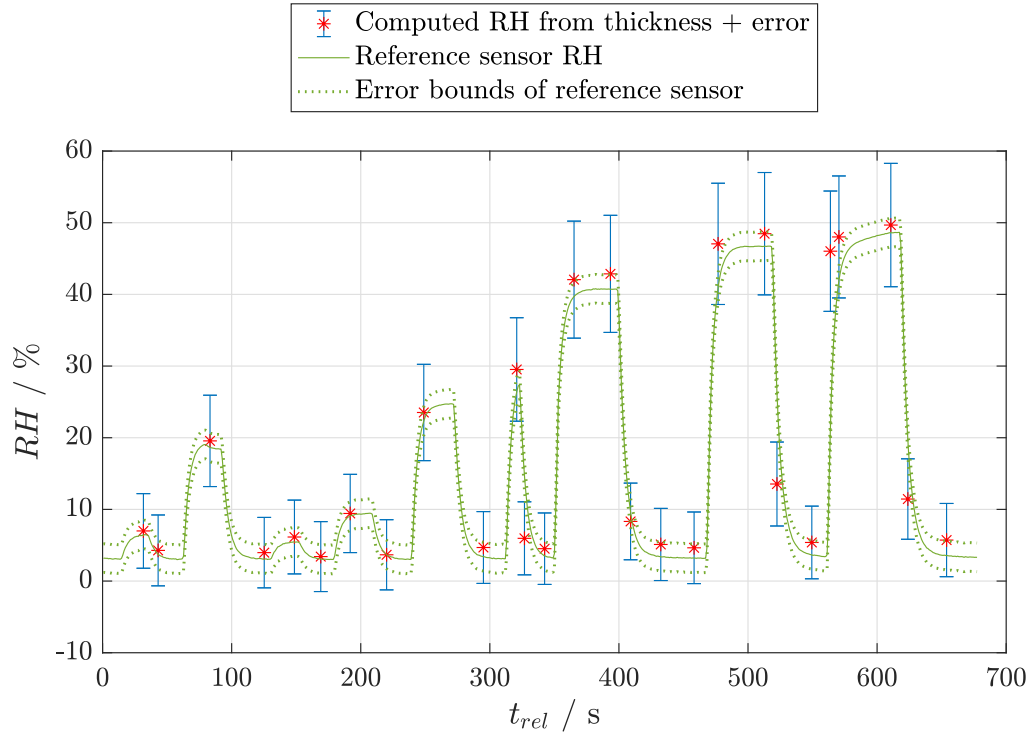

Figure 31: Evaluation measurement 3: Comparison of RH values, computed with the thickness of the hydrogel and RH, measured with the reference humidity sensor. Error bars are determined with equation (40) and the uncertainties for the actual thickness measurement. The uncertainty of the reference sensor is $\pm 2\,\%$ [34].

Figure 32 is the result of the last measurement with the thin film of deposition sample no. 2, because in the end it got damaged by dissolution at humidity levels greater than 97 %RH. Further measurements could not be performed anymore with that deposition. Nevertheless, it provides highly valuable data at $RH > 90$ %RH for the calibration of χ, described in section 6.3. The data below 90 %RH is not used for the calibration. It can be seen in figure 32, that the fast increase of the humidity during the first 70 s causes remarkable deviation of both measurements, even outside of the error. It can be assumed, that this is caused by the slower response of the reference sensor. Compared to the other measurements shown in this section, the error is much higher for some points. A deeper investigation shows, that the main contribution comes from the higher uncertainty of the thickness fit. Somehow the quality of the white light interference pattern and hence also of the fit is decreased for this measurement. This could be caused by any environmental influence at the sample, that perturbed the thin film, like generation of additional interfaces.
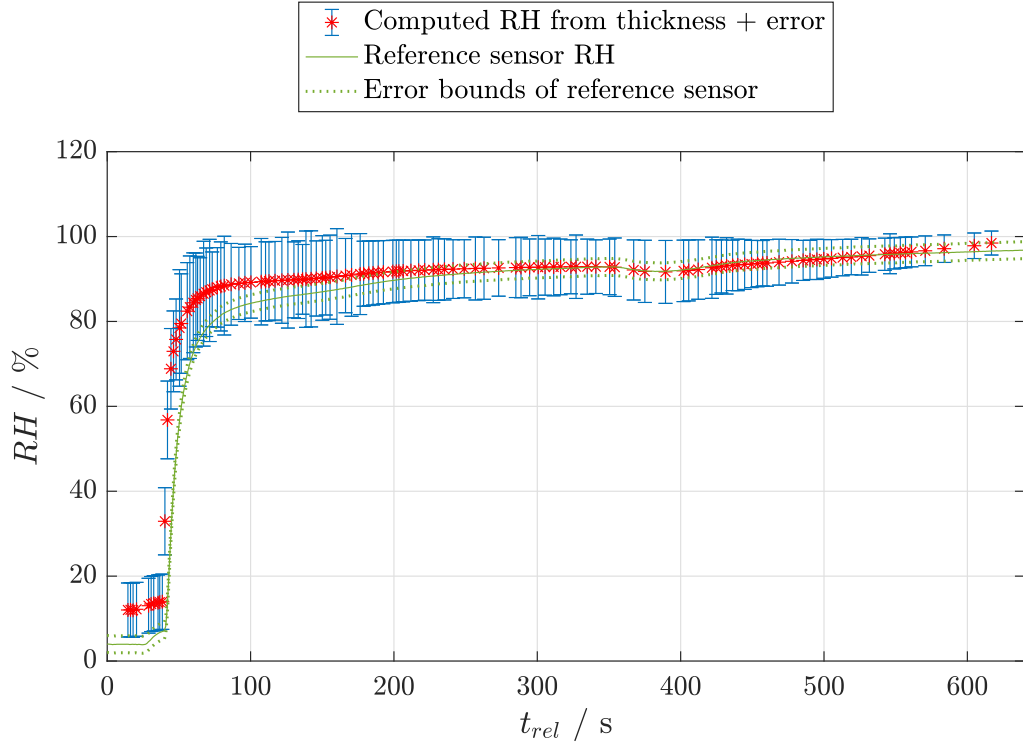

Figure 32: Evaluation measurement 4: Comparison of RH values, computed with the thickness of the hydrogel and RH, measured with the reference humidity sensor. Error bars are determined with equation (40) and the uncertainties for the actual thickness measurement. The uncertainty of the reference sensor is ± 2 % [34].

7 Conclusion and Outlook

Considering that the measurement setup is built from scratch and the early stage of the whole project, the final results of this thesis shown in section 6.4 are satisfying. It can be concluded that the proof of concept is successful and a realization of a humidity sensor, based on the proposed measurement principle, is realistic.

The created humidity generator works reliably and provides an adjustable relative humidity range from 3 %RH to 97 %RH, measured with the reference humidity sensor. Furthermore, it is possible to investigate the response times of the applied sensors, because the high volume flow offers the possibility of dynamic changes of RH under a second. The stability of the RH setting is sufficient within ± 2 %RH. While the measurements it is observed, that the valve releases the steam periodically. Obviously, pressure needs to be built to overcome the spring of the valve. This effect could be minimized with the application of a check valve with a softer spring. At high RH levels (> 85 %RH) the humidity setting starts to drift slightly. It is assumed, that the hot steam heats up the cooler and already condensed water starts to evaporate again, which increases RH. This effect could be minimized, if the cooler would work more efficiently. For example, the PTFE tube could be placed within a cold water bath, rather than in air. These are possible improvements for the future, but for the performed measurements the actual setup was sufficient.

According to former measurements it was already assumed, that the response of the thickness change of the hydrogel would be quite fast. The evaluation shows a significantly faster response of the hydrogel sensor, compared to the reference humidity sensor, which is the fastest commercially available. The result for the time constant, that is a measure for the response time, is for the hydrogel sensor $\tau_{63,pow} = (1.5 \pm 0.5)\,\mathrm{s}$ for the signal rise and $\tau_{63,pow} = (2.5 \pm 0.5)\,\mathrm{s}$ for the signal drop of about 44 %RH. These times are much faster than for the reference sensor ($\tau_{63,ref} = (6.2 \pm 0.5)\,\mathrm{s}$ for the rise and $\tau_{63,ref} = (7.8 \pm 0.5)\,\mathrm{s}$ for the drop). Hence, there is great potential for future applications, that require humidity detection with fast response times.

Section 6.4 shows, that all RH values, derived with the optical hydrogel setup, match the RH values, measured with the reference humidity sensor, within their error bars. This calculation of the RH value from the hydrogel sensor is enabled by the Flory Huggins parameter χ, that is empirically determined for the applied pHEMA thin film composition. It can be concluded, that the white light interference setup, which was evaluated for these measurements, works out pretty well. The model curve of the self-developed algorithm, that fits the thin film thickness according to the theoretic interference pattern, matches well with the measured spectra. The quality of the fit decreases just at very high humidity levels, which results in a higher uncertainty of the fitted thickness values. Fit data with a high MSE ($>$ 20) is not considered for the evaluation. For determination of thicknesses in that extreme humidity range, the refractive index could be fitted additionally. Therefore, spectra at different incident angles ought to be recorded, but the thickness must stay constant for all those measurements. This would be almost impossible, because in that range already tiny fluctuations of RH cause a huge variation of the

thin film thickness. The afford to perform measurements in that range would be far too high, especially because dissolution already starts at that high RH regime and destroys the thin film anyway. For a later application with a non-soluble material composition, that swells less according to Unger et. al. [13], it is assumed that also the refractive index stays constant over the whole RH range. Thus, the defined interference model should be entirely applicable.

The evaluation of the measured data yields some weak spots of the actual measurement setup. For this proof of concept, a pure pHEMA thin film without any additional crosslinker is chosen, because it provides the highest swellability. However, the swelling is hardly detectable at low RH values. An increase of the humidity from 3 %RH to 6 %RH yields to a thickness increase of about 1.5 nm, which is 0.2 % of the initial thickness. One the other hand the overall swelling is much higher than expected (about $+100$ percent with respect to the initial thickness), especially because of the immense increase at high humidity levels. This swelling behavior provides high sensitivity at humidities > 70 %RH of the measurement system, but depending on the application the whole RH range is relevant. Thus, a material composition with a flatter swelling curve would be preferable.

For an industrial application, the laser interference setup would be still the measurement principle of choice. The parts needed for this setup could be produced quite cheap, whereas for the white light interference a spectrometer is needed, which would be rather expensive. However, this measurement principle has some major drawbacks in the actual configuration with a pure pHEMA thin film. For an initial thickness of about 630 nm, the high swelling leads to an increase over about two periods of the interference pattern (cf. figure 22). Thus, the relation between the reflected laser power and the film thickness is ambiguous. In the actual configuration, the setup would not be practically applicable, because a calculation of a distinct RH value from a measured laser power is not possible. This problem could be overcome with a thinner initial thickness and a material composition, that swells less. Also the application of a near-infrared laser would help to stretch the interference pattern and extend the range, in which an unambiguous mapping is possible.

Furthermore, the reflection at the initial interface together with an incident angle, that deviates slightly from its nominal value, cause a shift of the ideal interference pattern. This shift could be evaluated with a simultaneous measurement of the absolute thickness (figure 22). Since the substrate thickness can vary within an uncertainty, this shift would be unique for every single sensor, which complicates an industrial application.

A possible strategy to overcome this problem is the application of a fiber. If the hydrogel thin film is deposited directly onto the tip of a fiber, this initial interface between air and the backside of the substrate can be avoided. A setup with the coated fiber is already realized and described in section 4.3.3. First attempts are already performed, but a detailed evaluation is task of an ongoing project. In this proposed project, the system should record humidity within concrete walls to estimate corrosion. Such a harsh environment causes problems for commercial sensors. This implementation has the big advantage, that all electronic parts are far away from the actual measurement position. Furthermore, it provides the advantage, that a measurement network can be realized and still be read out with just one detector.

The spatial allocation can be realized by a time of flight evaluation. Also humidity sensing in explosive environments would be possible, where electronic parts are restricted. Monitoring of water in gas pipelines is a possible application and topic of future work.

A second strategy is the application of a low coherent light source, like a LED for example. If the coherence length of the illuminating light source is below the substrate thickness, interference with light, that gets reflected at the initial interface, vanishes. An implementation is also topic of a future project.

In general, the stability of the measured laser power signal could be improved by implementation of a setup, that works not with the measurement of an absolute light power. By measuring a relative difference of the power of at least two light sources with different wavelengths, fluctuations caused by any source do not play a role. This is a general advantage of a relative measurement. The white light interference approach is an example for such a strategy. Fluctuations of the light intensity do not bother the thickness fit, because this information just depends on the shape of the spectrum. Hence, this strategy would be somehow a combination of the two applied measurement techniques.

Also completely different measurement principles have been tested. The hydrogel thin film got deposited on top of two electrodes in an electronic circuit and the capacitance was measured. The non-linearity was even more distinct, compared to the optical measurements. Below 70 %RH a difference of the capacitance was hardly resolvable. Thus, it is recommended, that further developments should focus on the optical approach.

References

[1] José L. Lozán, Ludwig Karbe, and Ulrich Neukirch. Wasser als Grundlage des Lebens. *Warnsignal Klima: Genug Wasser für alle?*, pages 21–30, 2011.

[2] Stanislav A. Kolpakov, Neil T. Gordon, Chengbo Mou, and Kaiming Zhou. Toward a new generation of photonic humidity sensors. *Sensors (Switzerland)*, 14(3):3986–4013, 2014.

[3] Robert H. Perry, Don W. Green, and James O. Maloney. *Chemical Engineers ' Handbook*. McGraw-Hill, 7th edition, 1997.

[4] John M. Wallace and Peter V. Hobbs. *Atmospheric science, an introductory survey*. Elsevier, Oxford, 2 edition, 2006.

[5] John W. Draper. *A Text-book on Chemistry*. Harper & Brothers, New York, 1861.

[6] Der Hygrograph – ein präzises Messinstrument. https://www.brune.info/magazin/thermo-hygrographen/ [Online. Last accessed: 2017-11-12].

[7] World Meteorological Organisation. Guide to Meteorological Instruments and Methods of Observation. https://library.wmo.int/pmb_ged/wmo_8_en-2012.pdf [Online. Last accessed: 2017-11-14].

[8] Arnold Wexler and Richard W. Hyland. *The NBS standard hygrometer*. Natianal Bureau of Standards, Washington D.C., 1964.

[9] Denes K. Roveti. Choosing a humidity sensor: A review of three technologies. *Sensors (Peterborough, NH)*, 18:54–58, 2001.

[10] Sensirion. Datasheet SHT3x-DIS. https://www.sensirion.com/fileadmin/user_upload/customers/sensirion/Dokumente/2_Humidity_Sensors/Sensirion_Humidity_Sensors_SHT3x_Datasheet_digital.pdf [Online. Date accessed: 2017-11-18].

[11] Benjamin Lang and Alexander Bergmann. Design Framework for a Gas Sensor Based on an Open Photoacoustic Resonator. *Sensors, 2016 IEEE*, pages 106–109, 2016.

[12] A. H. M. Habib Ahsan, Carlos F. Lange, and Walied Moussa. Development of a humidity microsensor with thermal reset. *Proceedings - International Conference on MEMS, NANO and Smart Systems, ICMENS 2003*, pages 89–93, 2003.

[13] Katrin Unger, Roland Resel, and Anna M. Coclite. Dynamic Studies on the Response to Humidity of Poly (2-hydroxyethyl methacrylate) Hydrogels Produced by Initiated Chemical Vapor Deposition. *Macromolecular Chemistry and Physics*, 217(21):2372–2379, 2016.

[14] IUPAC. *Compendium of Chemical Terminology - Gold Book*. Blackwell Scientific Publications, Oxford, 2014.

[15] Michael Rubinstein and Ralph H. Colby. *Polymer Physics*. Oxford University Press, 2003.

[16] Xiaodong Chen and Harald Fuchs. *Soft Matter Nanotechnology: From Structure to Function*. Wiley-VCH, Weinheim, 2015.

[17] Enas M. Ahmed. Hydrogel: Preparation, characterization, and applications: A review. *Journal of Advanced Research*, 6(2):105–121, 2015.

[18] Martin Gellman and Joel Hirsch. Comparison of soflens contact lenses (polymacon) with hard contact lenses and spectacles. *American journal of optometry and physiological optics*, 52:128–133, 1975.

[19] Ranjita K. Bose and Kenneth K. S. Lau. Initiated CVD of Poly(2-Hydroxyethyl Methacrylate) Hydrogels: Synthesis, Characterization and In-vitro Biocompatibility. *Chemical Vapor Deposition*, 15(4-6):150–155, 2009.

[20] Jui-Yang Lai, Tsu-Pin Wang, Ya-Ting Li, and I-Hao Tu. Synthesis, characterization and ocular biocompatibility of potential keratoprosthetic hydrogels based on photopolymerized poly(2-hydroxyethyl methacrylate)-co-poly(acrylic acid). *Journal of Materials Chemistry*, 22(5):1812–1823, 2012.

[21] J. Jaczewska, I. Raptis, A. Budkowski, D. Goustouridis, J. Raczkowska, M. Sanopoulou, E. Pamuła, A. Bernasik, and J. Rysz. Swelling of poly(3-alkylthiophene) films exposed to solvent vapors and humidity: Evaluation of solubility parameters. *Synthetic Metals*, 157(18-20):726–732, 2007.

[22] Iwao Teraoka. *Polymer Solutions*. John Wiley & Sons, New York, 2002.

[23] Achim Trogisch and Uwe Franzke. *Feuchte Luft - h,x-Diagramm: Praktische Anwendungs- und Arbeitshilfen*. VDE-Verlag, Berlin, 2012.

[24] Arden L. Buck. New Equations for Computing Vapor Pressure and Enhancement Factor, 1981.

[25] Bernd Glück. *Zustands- und Stoffwerte*. Verlag für Bauwesen, Berlin, 1991.

[26] Albert Perot and Charles Fabry. On the Application of Interference Phenomena to the Solution of Various Problems of Spectroscopy and Metrology. *Astrophysical Journal*, 9:87, 1899.

[27] Eugene Hecht. *Optics*. Pearson, Essex, 5th edition, 2017.

[28] Swapan K. Saha. *Principles of Interference*, pages 31–49. Springer, New York, 2011.

[29] Tuan Vo-dinh. *Biomedical Photonics Handbook*. CRC Press, Boca Raton, 2003.

[30] Anna M. Coclite, Rachel M. Howden, David C. Borrelli, Christy D. Petruczok, Rong Yang, Jose Luis Yagüe, Asli Ugur, Nan Chen, Sunghwan Lee, Won Jun Jo, Andong Liu, Xiaoxue Wang, and Karen K. Gleason. 25th Anniversary Article: CVD polymers: A new paradigm for surface modification and device fabrication. *Advanced Materials*, 25(38):5392–5423, 2013.

[31] Francis A. Jenkins and Harvey E. White. *Fundamentals of Optics*. McGraw-Hill, New York, 3rd edition, 1957.

[32] Thunder Scientific. Datasheet Model 9500 - Automated "Two-Pressure" Humidity Generator. http://www.thunderscientific.com/humidity_equipment/9500-System-Specs-2016-05.pdf [Online. Date accessed: 2018-01-02].

[33] aDROP - Direktverdampfer aSTEAM DV-4 Series Produktbeschreibung. http://www.adrop.de/de/Produkte/verdampfer_aSTEAM/index.php [Online. Date accessed: 2018-01-02].

[34] Sensirion - How to Understand Specification of Relative Humidity Sensors. https://www.sensirion.com/fileadmin/user_upload/customers/sensirion/Dokumente/2_Humidity_Sensors/Sensirion_Humidity_Sensors_Specification_Statement.pdf [Online. Date accessed: 2018-01-28].

[35] David R. Lide. *CRC Handbook of Chemistry and Physics*. CRC Press, 87th edition, 2007.

[36] Irving H. Malitson. Refraction and Dispersion of Synthetic Sapphire. *Journal of the Optical Society of America*, 52(12):1377–1379, 1962.

[37] Sensirion - Testing Guide For SHTxx Relative Humidity & Temperature Sensors. https://www.sensirion.com/fileadmin/user_upload/customers/sensirion/Dokumente/2_Humidity_Sensors/Sensirion_Humidity_Sensors_Testing_Guide.pdf [Online. Date accessed: 2018-01-22].

[38] Paul Salzmann, Alberto Perrotta, and Anna M. Coclite. Different response kinetics to temperature and water vapor of acrylamide polymers obtained by initiated Chemical Vapor Deposition. *ACS Applied Materials*, 2018.

[39] James Mark. *Physical Properties of Polymers Handbook*. Springer, New York, 2nd edition, 2006.

[40] Allan F. M. Barton. *Handbook of Polymer-Liquid Interaction Parameters and Solubility Parameters*. CRC Press, Boca Raton, 1990.

[41] CROW Polymer Properties Database - Temperature and concentration dependence of interaction parameter. http://polymerdatabase.com/polymer physics/Chi Temp dependence.html [Online. Date accessed: 2018-01-24].